



SELF-ORGANIZING LOW TO HIGH CONFINEMENT TRANSITIONS IN TOKAMAK PLASMAS

P. N. GUZDAR

**INSTITUTE FOR RESEARCH IN ELECTRONICS AND APPLIED
PHYSICS (IREAP)
UNIVERSITY OF MARYLAND**

**AUTUMN COLLEGE ON PLASMA PHYSICS: LONG LIVED
STRUCTURES AND SELF-ORGANIZATION IN PLASMAS
TRIESTE, ITALY**

**IN COLLABORATION WITH R.G. KLEVA , UMD, USA
A. DAS AND P. K. KAW, IPR GANDHINAGAR, INDIA
N. CHAKRABARTI, SINP, KOLKATA, INDIA
R.J. GROENBER AND P. GOHIL,**

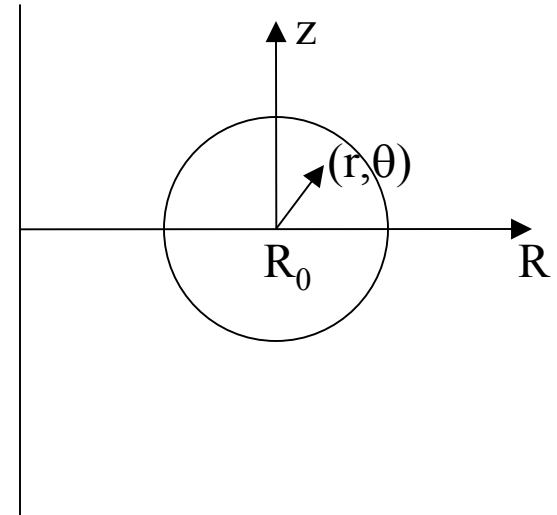
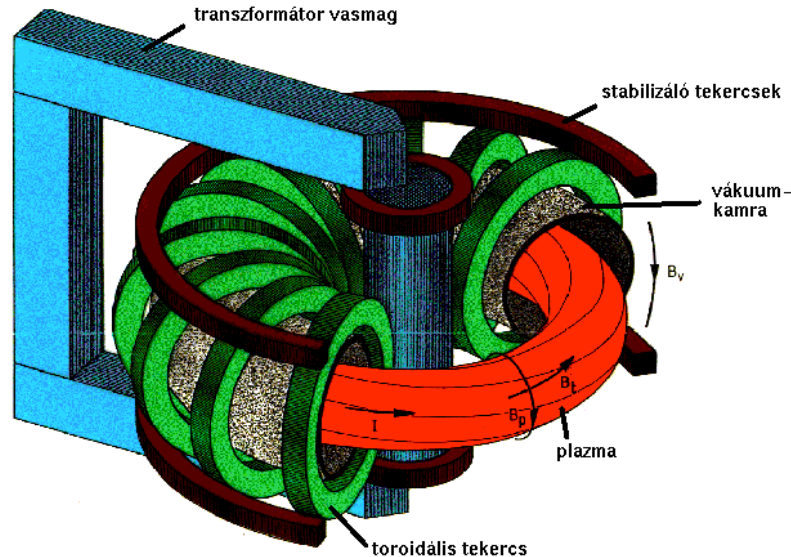


OUTLINE OF THE TALKS

- GENERAL INTRODUCTION
- EXPERIMENTAL OBSERVATIONS
- SIMULATION RESULTS
- THEORETICAL MODEL
- COMPARISON WITH EXPERIMENTS
- CONCLUSIONS

TOKAMAK

“TOroidalnaya”, “KAmera”, “MAgnitnaya”
 “Katushka”



$$B_T = B_{0T} R_0 / R$$

$$B_{0T} / (1 + r \cos(\theta) / R_0)$$

$$\mathbf{B} = \mathbf{e}_\phi B_T + \mathbf{e}_\theta B_P$$

$$q = r B_T / R B_P$$

COMBINATION OF TOROIDAL AND POLOIDAL FIELDS CREATE MAGNETIC SURFACES
 IF q IS IRRATIONAL.
 FIELD LINES CLOSE ON THEMSELVES IF $q = m/n$. SUCH SURFACES ARE CALLED RATIONAL
 SURFACES



TOKAMAK WITH DIVERTOR

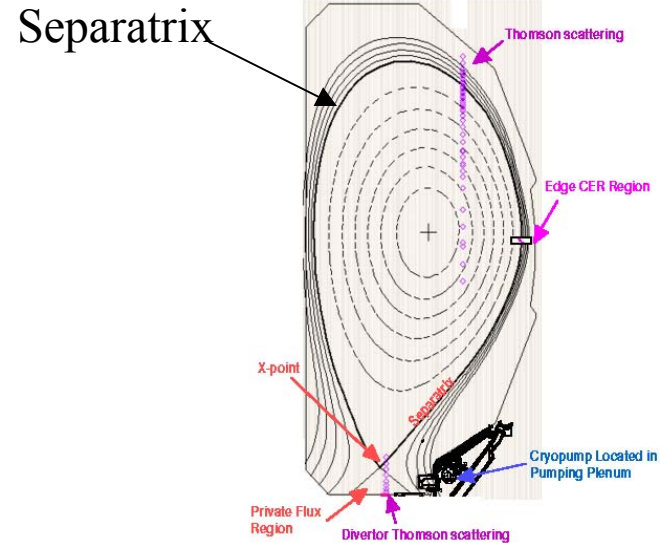
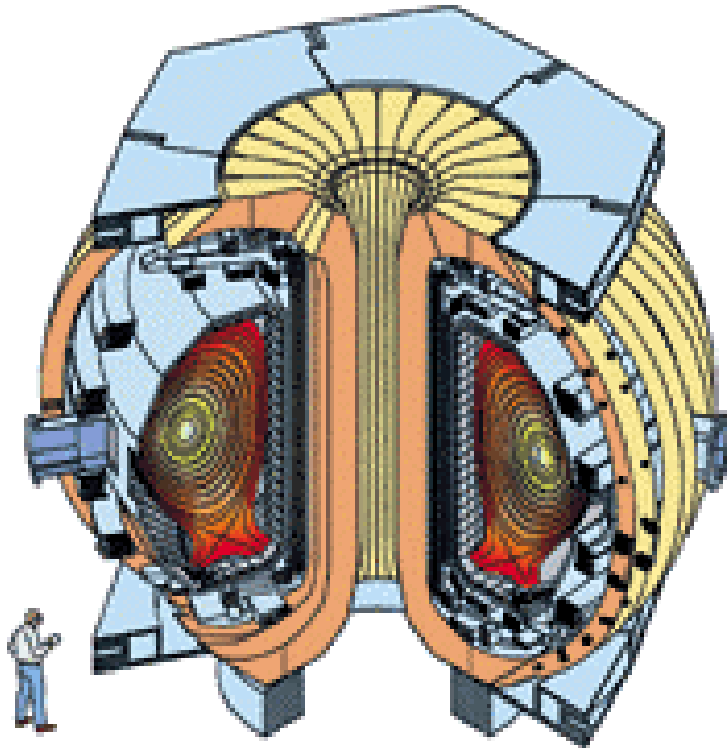


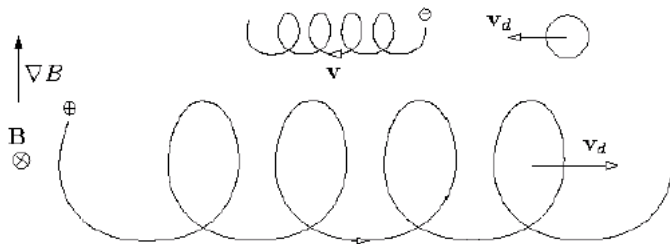
FIG. 1. A cross section of the DIII-D vacuum vessel with a flux contour plot of a typical lower single-null diverted plasma configuration is shown along with the locations of the Thomson scattering and CER measurements.

ADVANTAGE OF DIVERTOR: OUTFLOW OF PLASMA ACROSS SEPARATRIX DRAINED ALONG FIELD LINES TO DISTANT DIVERTOR PLATE. REDUCED INFLUX OF IMPURITIES FROM WALL.



PARTICLE ORBITS

Grad B Drift



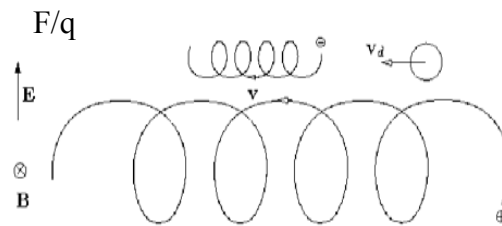
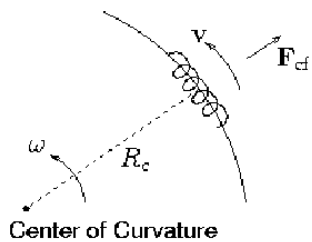
$$V_{\nabla B} = \frac{1}{e} \frac{mv_{\perp}^2}{2B} \frac{\vec{B} \times \nabla B}{B^2}$$

Curvature Drift

$$V_{DF} = \frac{1}{q} \frac{\vec{F} \times \vec{B}}{B^2}$$

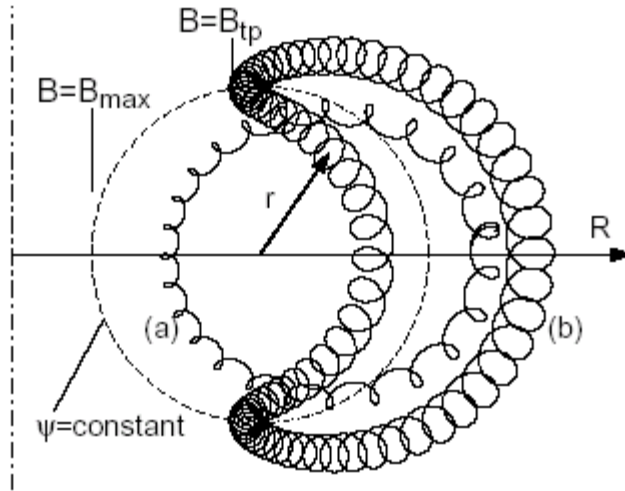
$$F_c = \frac{mv_{\parallel}^2}{R_c^2} \vec{R}_c \quad \frac{\vec{R}_c}{R_c^2} = -(\hat{b} \cdot \nabla) \hat{b} \quad \hat{b} = \frac{\vec{B}}{B}$$

$$v_c = \frac{1}{e} mv_{\parallel}^2 \frac{\vec{B} \times (\hat{b} \cdot \nabla) \hat{b}}{B^2}$$





MAGNETIC CONFINEMENT -PARTICLE ORBITS



- (a) Circulating particles
- (b) Trapped particles

$$E = \frac{1}{2} m(v_{\perp}^2 + v_{\parallel}^2) = \mu B + \frac{1}{2} m v_{\parallel}^2$$

$$v_{\parallel} = \pm \sqrt{E - \mu B}$$

$E < \mu B$ trapped particles

$E > \mu B$ circulating particles

$$\vec{B}_p = \nabla \psi \times \mathbf{e}_{\phi} / R$$

Toroidal canonical momentum conservation

$$\left(m v_{\text{tor}} - \frac{q A_{\phi}}{c} \right) R = \text{Const} = m R v_{\text{tor}} - \frac{q}{c} \psi$$

$$\Delta r = 2 \frac{m R v_{\parallel} c}{q \frac{\partial \psi}{\partial r}} = 2 \frac{m v_{\parallel} c}{q B_p}$$



WHAT ARE LOW-HIGH TRANSITIONS ?

- Before 1982, auxiliary heating of tokamak plasmas showed that energy confinement **deteriorated** with increase of power (Low or L- mode) -dismal prospects for fusion
- ASDEX (**A**xi**S**ymmetric **D**ivertor **E**Xperiment) showed that beyond a critical power the discharge made a transition to a good confined state with the energy confinement improving by 3-4 (High or H-Mode) (Phew !!)
- This transition from Low to High Confined mode is called L-H transitions
- L-H transitions characterized steep gradients of density and temperature in the edge region indicating an edge transport barrier
- In the recent past NEW enhanced confinement modes have been found with transport barriers in the core

Ref: J. W. Conner and H. R. Wilson, “A review of the L-H transition” Phys. Plasmas and Control. Fusion **42**, R1-R74, (2000).

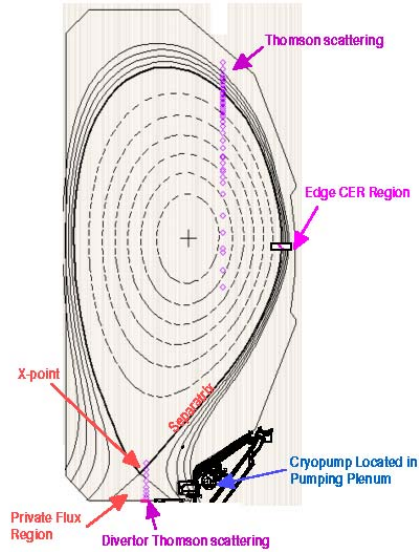


FIG. 1. A cross section of the DIII-D vacuum vessel with a flux contour plot of a typical lower single-null diverted plasma configuration is shown along with the locations of the Thomson scattering and CER measurements.

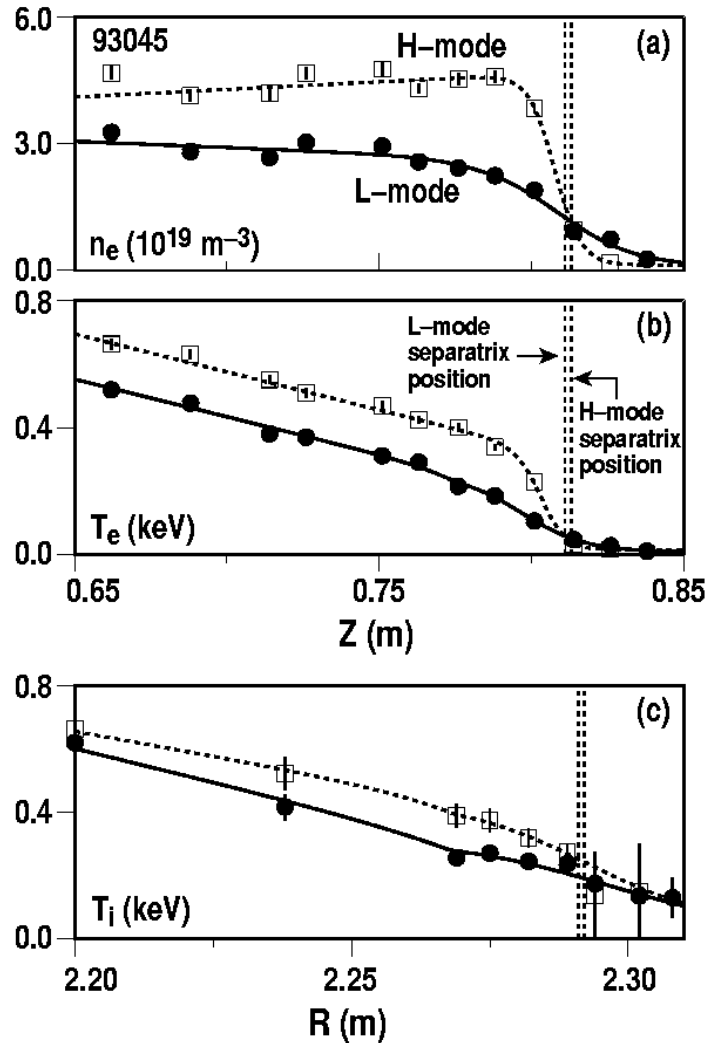


FIG. 2. Typical edge profiles of (a) n_e , (b) T_e , and (c) T_i for L-mode (dots) and H-mode (squares). The curves are modified hyperbolic tangent fits to the data. The vertical lines show the separatrix position.



MOYER ET AL., PHYS. PLASMAS, 2, 2397 (1995) HAHM AND BURRELL, 2, 1648 (1995)

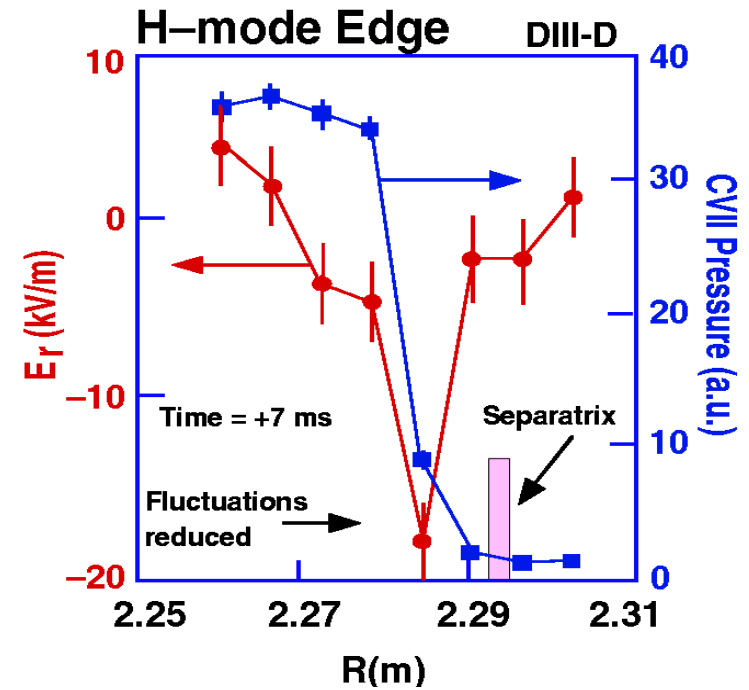
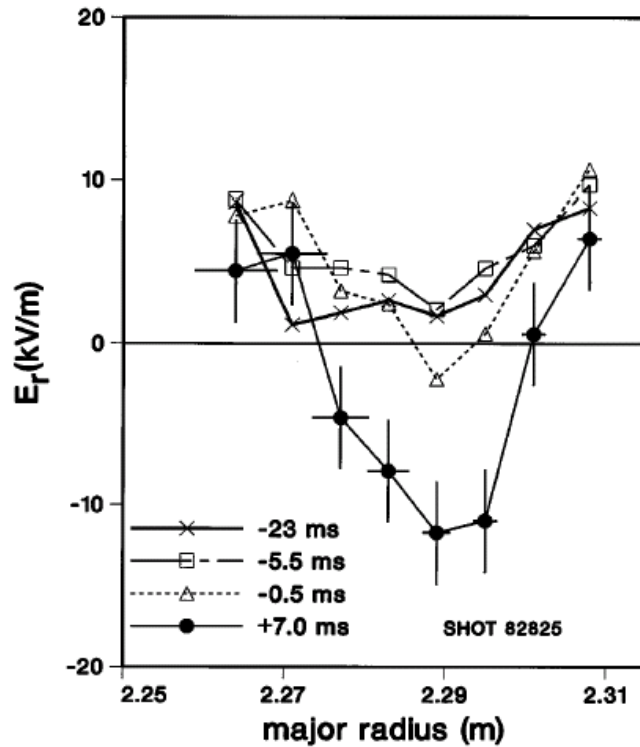


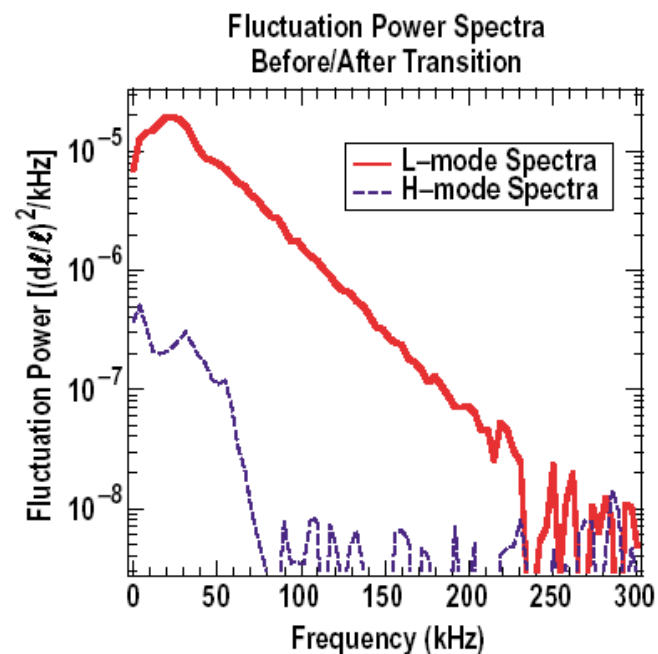
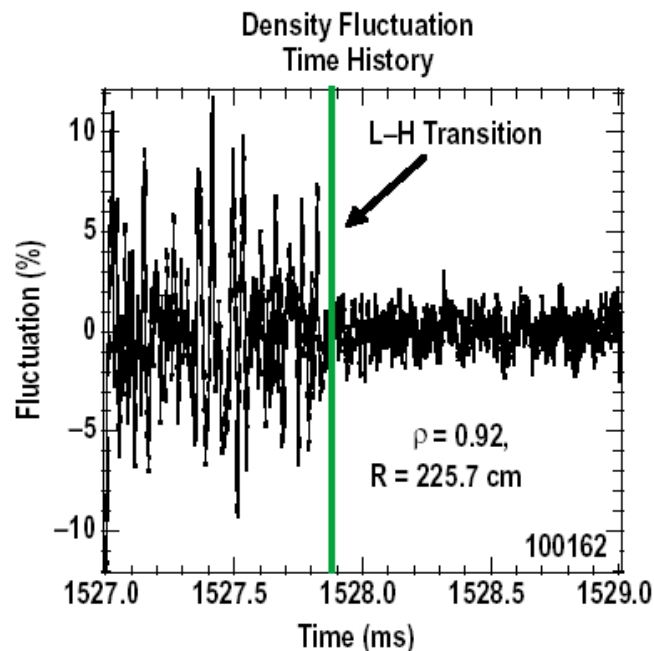
Figure 6. Temporal evolution of steep gradients in the radial electric field, E_r , for shot 82825 from DIII-D [54]; times are measured relative to the L-H transition.

$$E_r = (Z_i e n_i)^{-1} \nabla P_i - v_{\theta i} B_\phi + v_{\phi i} B_\theta,$$



DRAMATIC REDUCTION IN TURBULENCE OBSERVED AT L-H TRANSITION

- BES fluctuation measurements obtained during L-H transition experiment at plasma edge, $\rho = 0.9-1.05$, 2-D array employed
- Fluctuation power decreases by roughly two orders of magnitude after transition



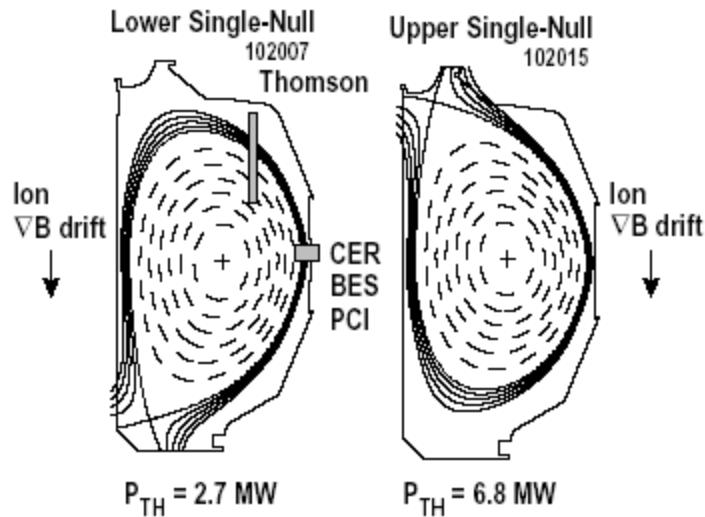


Fig. 1. Comparison of flux surface plots from EFIT for LSN and USN discharges. Also shown are the measurement locations for Thomson scattering (Thomson), charge exchange recombination spectroscopy (CER), beam emission spectroscopy (BES), and phase contrast imaging (PCI).

Power Threshold for L-H Transition

P_{th} for ∇B drift away from X point \sim
 $(2-8) \times P_{th}$ for ∇B drift towards X point



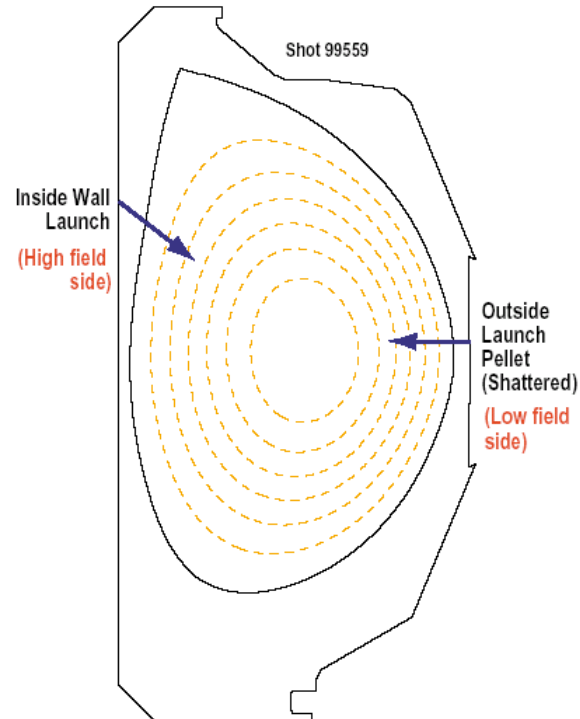
CARLSTROM ET. AL, NUCLEAR FUSION 39, 1941, (1999)

PELLETS WERE LAUNCHED FROM THE LOW FIELD SIDE OR HIGH FIELD SIDE OF DIII-D

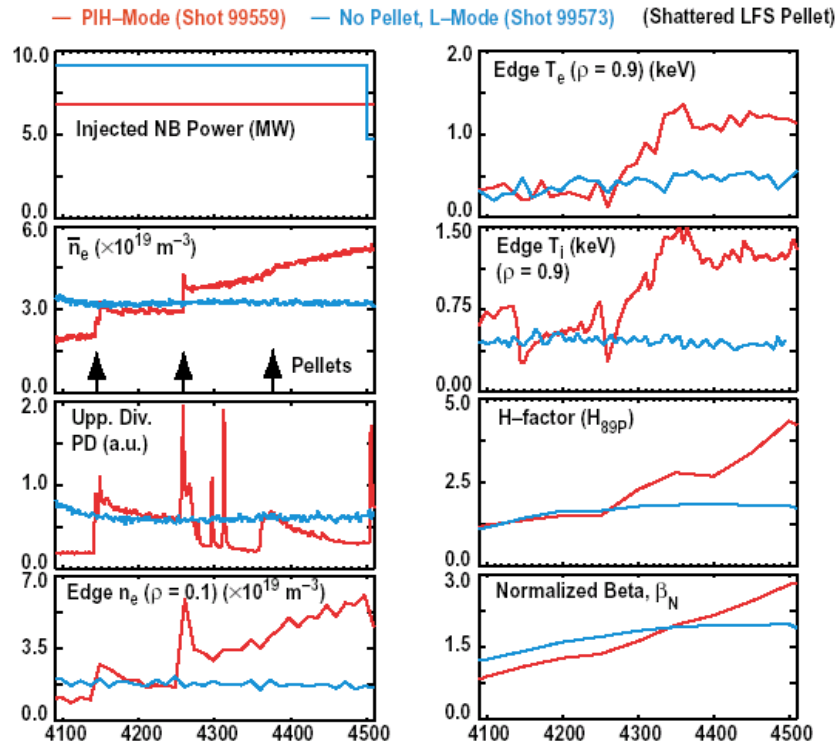
- Outside wall launched pellets (low field side) were shattered prior to entry into plasma in order to minimize pellet penetration \Rightarrow predominantly edge density perturbation
- Type: solid deuterium
Pellet size: 2.7 mm
Equivalent number of particles: 2×10^{20}
Rep rate: up to 10 Hz
Speed: 100–350 m s⁻¹
Speed for Specific Shots:

Shot

99559	314, 194 and 160 m s ⁻¹ (shattered pellets – outside launch)
100162	222 m s ⁻¹ (inside launch)
100170	235 m s ⁻¹ (inside launch)



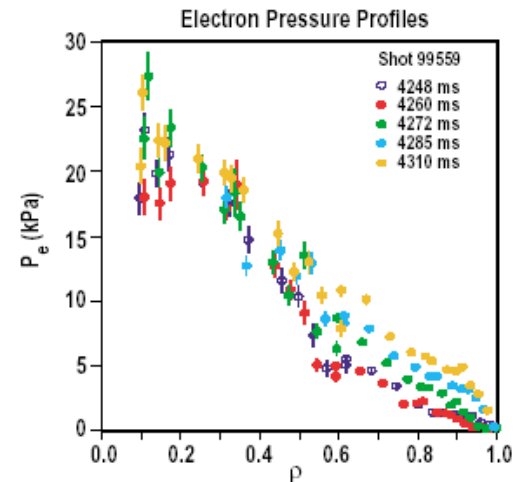
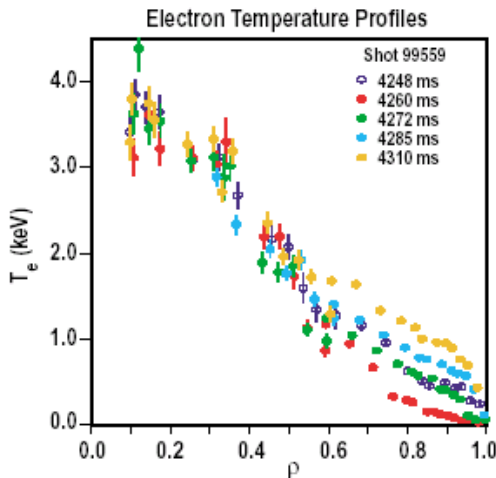
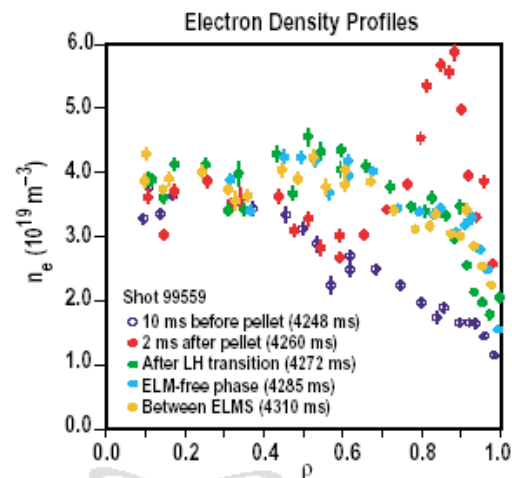
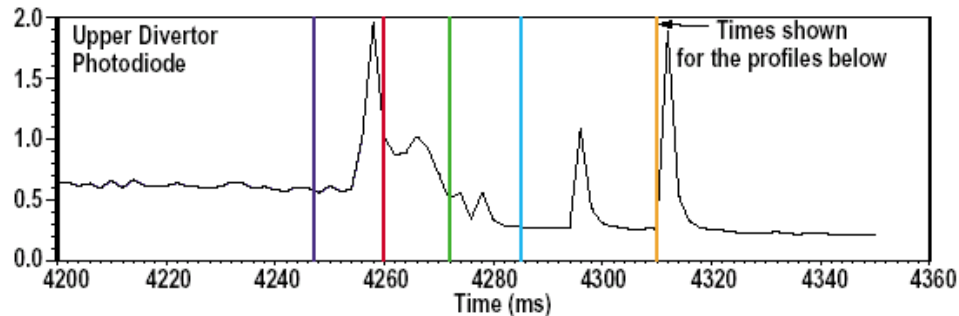
COMPARISON OF PIH-MODE DISCHARGE ($P_{\text{NBI}} = 6.8 \text{ MW}$) WITH NO PELLETS, L-MODE DISCHARGE ($P_{\text{NBI}} = 9.2 \text{ MW}$)



- The power required to access H-mode is reduced by at least 2.4 MW using pellet injection

EVOLUTION OF ELECTRON KINETIC PROFILES IN THE PELLET INDUCED H-MODE PLASMA

- The edge electron temperature is reduced at the L-H transition — disagrees with H-mode theories requiring edge critical electron temperature





OBSERVATIONS ON CCT

Taylor et al. PRL, 63, 2365 (1989)

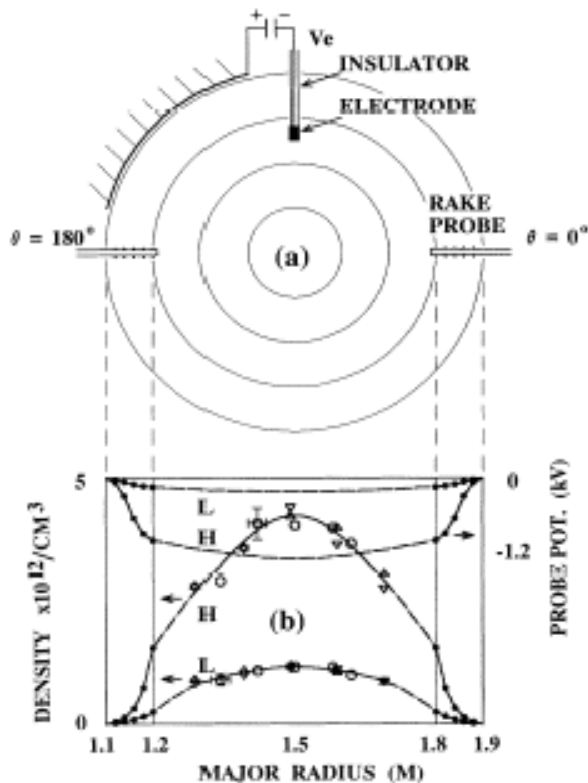


FIG. 1. (a) Cross section of tokamak, $a=40$ cm, showing the location of the exciting electrode, $r_e=25$ cm, and the "rake" probe arrays used for measuring floating potential and edge plasma density in the E -field layer. (b) Edge profiles of potential and density in L and H modes. The core density values are derived from Abel-inverted microwave interferometer data. Dashed lines represent best estimates of unmeasured floating potentials in the interior.

CCT parameters

$R=1.5$ m, $a=0.4$ m

$B_T=0.3$ T, $I_p=50$ kA

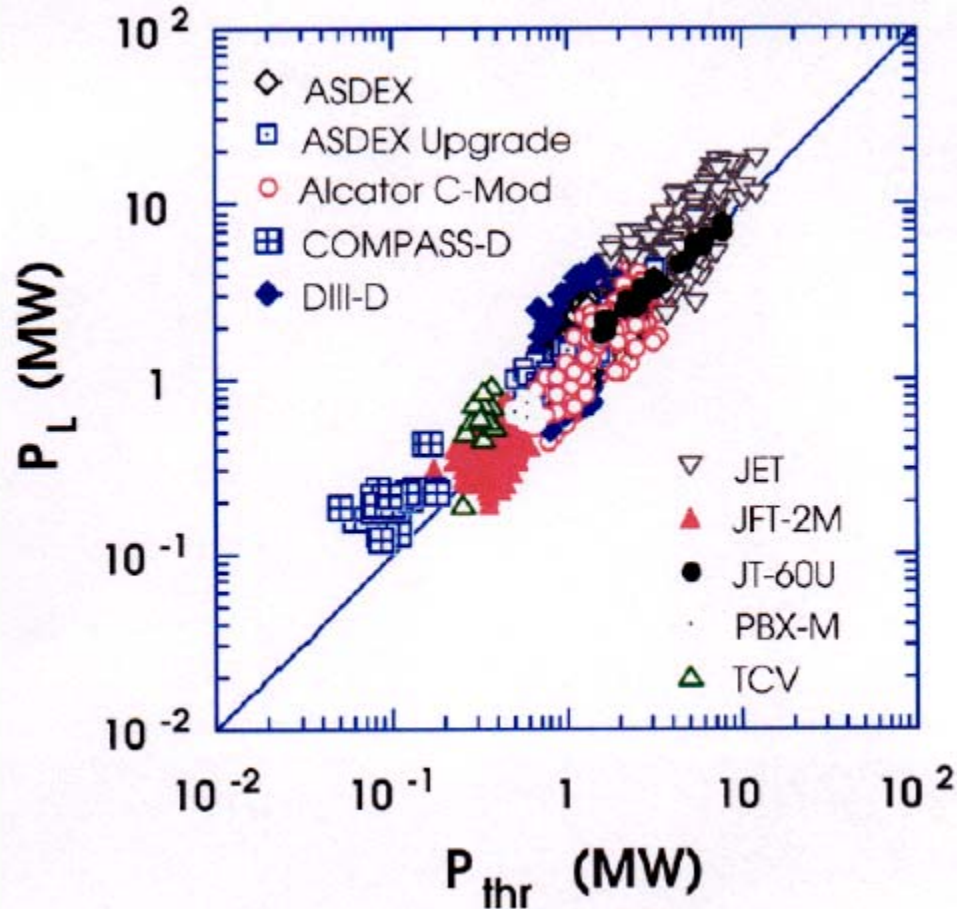
$N_e=5 \times 10^{12}/\text{cm}^3$

Transition occurs at critical value of electrode potential -200 V



Empirical scaling

T. Takizuka et al., Fusion Energy Proc. 16th Int. Conf. Montreal, 1996
(Vienna, IAEA), p 795, 1997

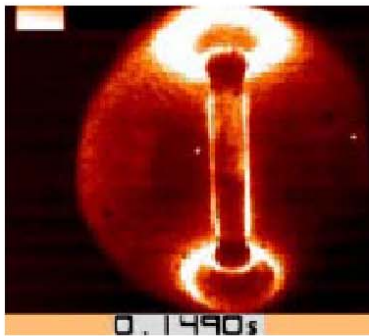


$$P_{th} = 0.45 B(T) n(10^{20} \text{m}^{-3})^{0.75} R(\text{m})^2$$

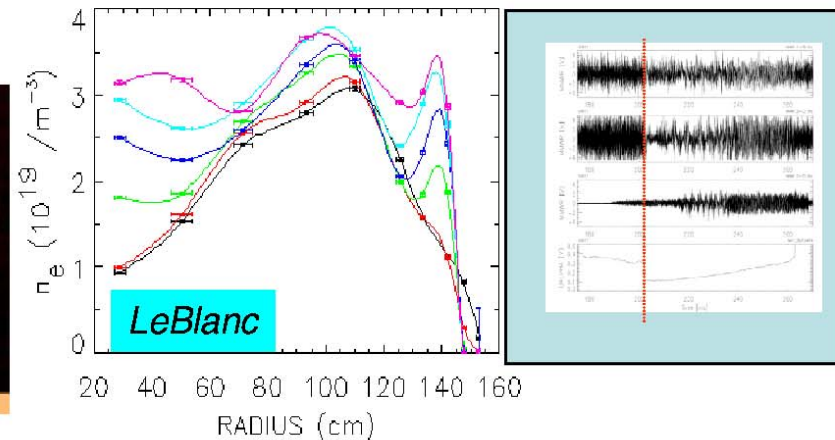
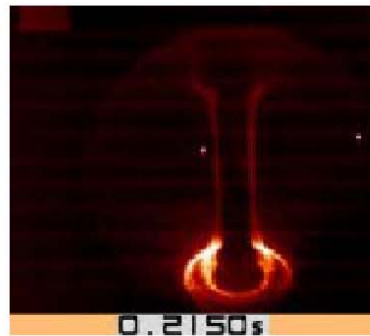
Bifurcations to enhanced plasma confinement state observed with both NBI and HHFW

Visible light, false color

Before transition



After transition



- NBI: Power required $\sim 10x$ that predicted from empirical scaling laws:
 - Strong magnetic shear?
 - Poloidal damping? Wall neutrals?

- Change in edge transport evident in density profile

- Fluctuations reduced at H mode transition

Edge reflectometry:
Peebles, Kubota (UCLA)

Fast camera: Maqueda (LANL)

H mode: Maingi, Bush (ORNL); LeBlanc

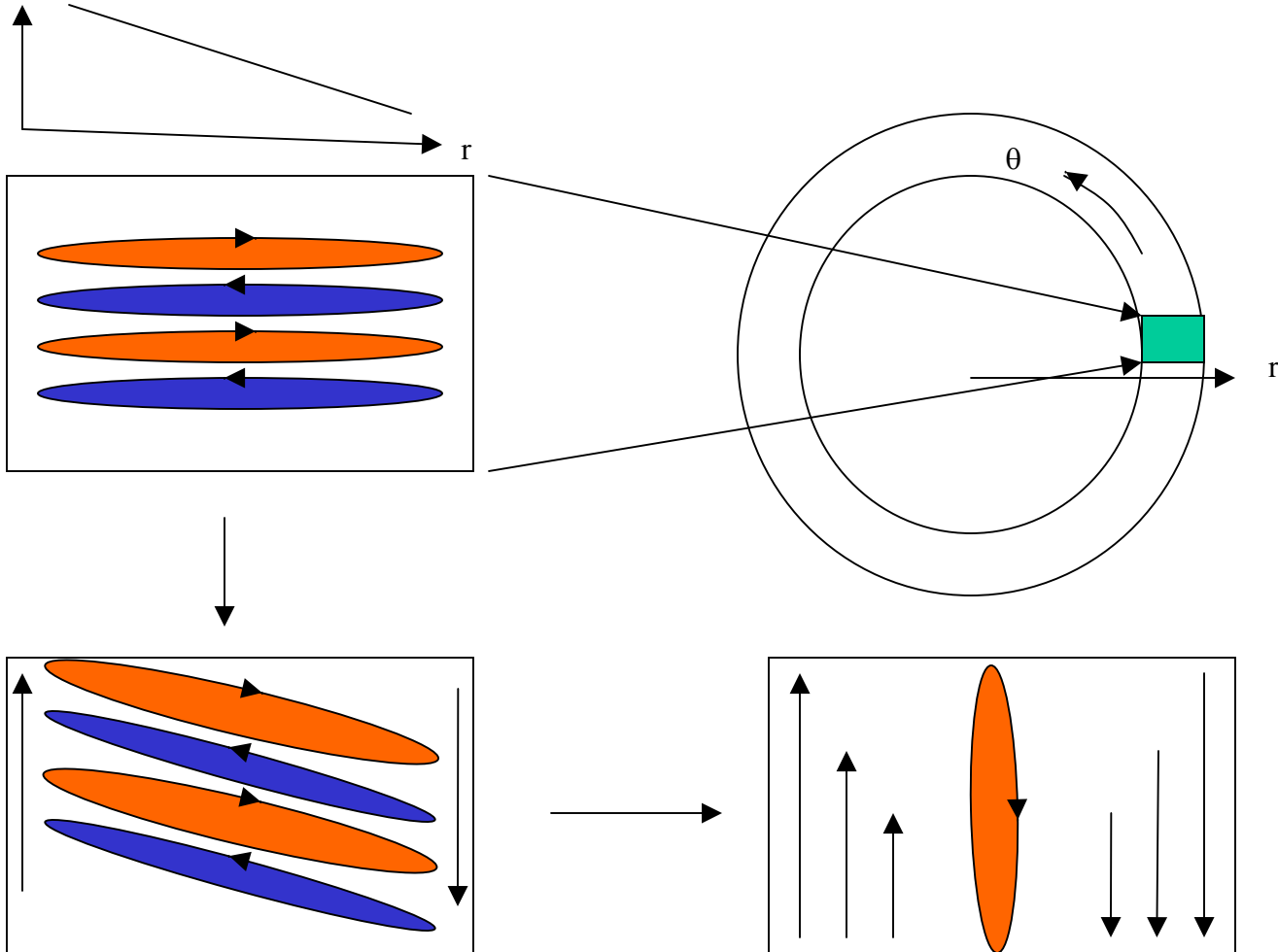


WHAT SHOULD THEORY/SIMULATIONS EXPLAIN ?

- What physics is responsible for L-H Transitions ?
- Why is the power threshold when ∇B drift is away from the X-point $2 - 8$ larger compared to the case when ∇B drift is towards the X-point ?
- Why does the pellet injection reduce the threshold power for the transition ?
- Can the same physics be playing a role in triggering an H-mode in tokamaks with an imposed electric field ?



WHY DOES SHEAR FLOW CREATE TRANSPORT BARRIER ?





THEORIES

- With DIII-D discovery of shear flow in the edge region
- Four classes of theories
 - Theories investigating shear/zonal flow generation instability mechanisms
The primary drive for the zonal flow is the fluctuations, generated shear flow in turn suppresses fluctuations
 - Assume shear flow exists how does it affect the turbulence and global transport ?
Model anomalous transport, $D = D_{NC} + D_a / [1 + (\omega_{ExB} / \gamma_0)]^{2n}$
Coupled transport equations for density or temperature and zonal/shear flow lead to bifurcated equilibria
 - Shear flows not driven by fluctuations but by variety of other mechanisms
 - Direct stabilization of source of L mode transport with increase of neutral beam power (no need for shear flow)



ZONAL FLOW INSTABILITY

Shear Flow Instability of Rayleigh-Benard Convection Vortices

1. L. N. Howard and R. Krishnamurty, *J. Fluid Mech.* **170**, 385, 1986.
2. K. B. Hermiz, P. N. Guzdar and J. M. Finn, *Phys. Rev. E* **51**, 325, 1995.

Shear Flow Instability of Driven Vortices

1. J. Drake, J. Finn, P. Guzdar, V. Shapiro, V. Shevchenko, F. Waelbroeck, A. Hassam, C. S. Liu and R. Sagdeev, *Phys. Fluids B*, **4**, 488, 1992.
2. J. M. Finn, J.F. Drake, P.N. Guzdar, *Phys. Fluids B* **4**, 2758, 1992.

Shear/Zonal flows driven by drift waves

- V. B. Lebedev, P. H. Diamond, V. D. Shapiro and G. I. Soloviev, *Phys. Plasmas* **2**, 4420 1995
- L. Chen, Z. Lin and R. White, *Phys. Plasmas Lett.*, **7**, 3129 (2000)
- F. Jenko, W. Dorland, M. Kotschenreuther and B. N. Rogers, *Phys. Plasmas*, **7**, 1904 (2000)
- P. K. Kaw and R. Singh, BAPS 1999 Centennial Meeting Atlanta Georgia, **44**, RP01, 109 (1999).
- A. I. Smolyakov, P. H. Diamond and M. Malkov, *Phys. Rev. Lett.*, **84**, 491 (2000).
- A. I. Smolyakov, P. H. Diamond and V. I. Shevchenko, *Phys. Plasmas*, **7**, 1349 (2000).



Coupled Transport and Zonal Flow Equations and Turbulence decorrelation

a) Anomalous Stringer Spin-Up

A. B. Hassam, T. M. Antonsen, Jr., J. F. Drake, and C. S. Liu, Phys. Rev. Lett. **6**, 309, (1991)

-Edge spin-up by poloidal asymmetry of anomalous particle transport $D = D_a(1 + \epsilon \cos(\theta))$. First Investigated by Stringer for neoclassical transport

b) Anomalous Viscosity

A. V. Rozhansky and M. Tendler, Phys. Fluids B **4**, (1992)

Anomalous neoclassical viscosity and ion inertia, driven by turbulent bifurcation behavior

c) ITG/Zonal flow

F. Hinton, G. Staebler, Phys. Fluids B, **5**, 1281 (1993)

B. Carreras et al., Phys. Plasmas **1**, 4018, (1994)

-Anomalous flow suppressed ion heat transport leads to bifurcation:

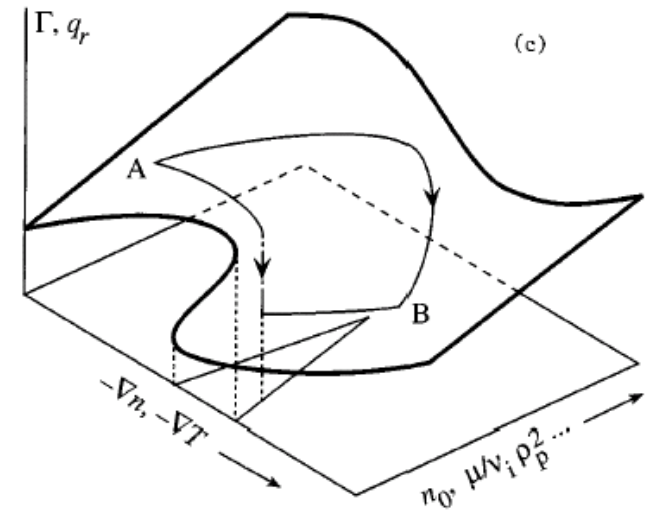
d) Decorrelation of Turbulence by Shear flows

H. Biglari, P. Diamond, and P. Terry, Phys. Fluids B **2**, 1 (1990)

Y. Z. Zhang and S. M. Mahajan, Phys. Fluids B **4**, 1385 (1992)

-How to describe the influence of weak and strong shear flow (shearing rate dV_θ/dx compared to growth rate) on fluctuations.

This can then be used to provide correct model of shear flow on reduced anomalous transport





Non-fluctuation driven shear flow non shear flow stabilization

a) Ion Orbit Loss (Neoclassical Theories)

Itoh, and K. Itoh, Phys. Rev. Lett. **60**, 2279, (1988)

K. C. Shaing and E. C. Crume, Phys. Rev. Lett. **63**, 2369, (1989)

-Ion Banana orbits much larger than electron banana orbits

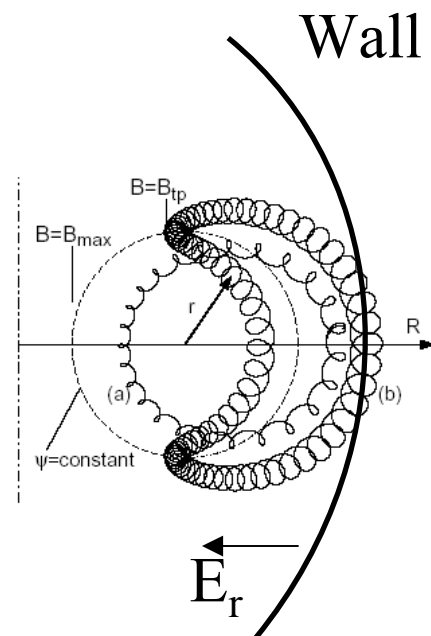
-In edge region ions lost preferentially, leading to a radial electric field on the scale of ion banana width providing shear flow

b) Two-fluid equilibria with flows

S. M. Mahajan, and Z. Yoshida, Phys. Plasmas **7**, 635 (2000)

Application of two fluid Double-Beltrami Equations to Edge

Characteristic scale of shear flow $\sim c/\omega_{pi}$





non-shear flow stabilization

Direct stabilization of instability responsible for L mode when heating power increase

a) Stabilization of finite β drift waves

O. Pogutse EPS 1997

W. Kerner et al. Contrib. Plasma Phys. **38**, 118 (1998)

No bifurcation just improved confinement

b) Stabilization of Peeling Modes (edge kink modes driven by bootstrap current)

H. R. Wilson et al., Plasma Phys. **4**, 1321 (1999)

Most complete and comprehensive review:

Ref: J. W. Conner and H. R. Wilson, “A review of the L-H transition”
Phys. Plasmas and Control. Fusion **42**, R1-R74, (2000).



CURRENT CODES

- THREE CODES, FINITE BETA REDUCED BRAGINSKII EQUATIONS
 - MARYLAND (ROGERS, DRAKE ZEILER CODE)
(flux tube code inside LCFS)
 - DALF (SCOTT)
(flux tube geometry, inside LCFS)
 - BOUT code
(couples regions inside and outside the separatrix regions)

All three codes address almost the same physics of toroidal drift-Alfven, resistive and 'ideal' ballooning modes, η_i modes and self-consistent shear flows BOUT has important additional SOL physics and coupling to inside LCFS.

Controversy:

MD code obtains self-consistent L-H transitions in two-dimensional parameter space (α_{MHD} , α_{D}) especially in which the density profile is allowed to evolve

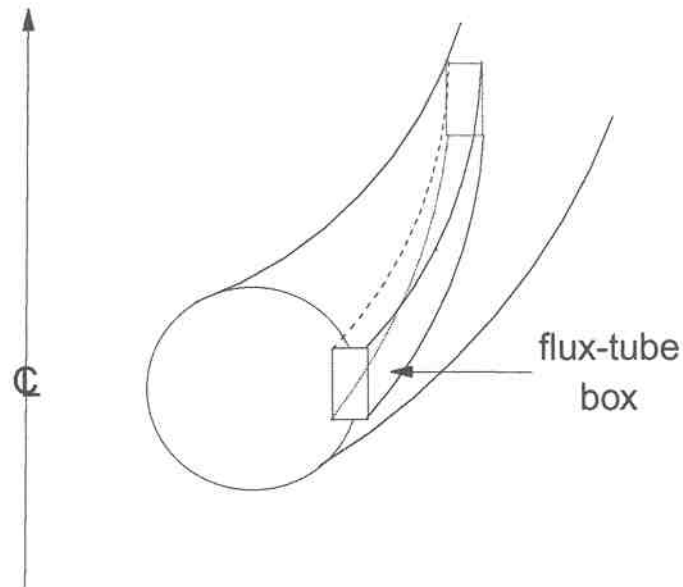
DALF Code shows no such self-consistent transition

BOUT code has potential for L-H transition with inclusion of profile evolution



3D SIMULATION GEOMETRY

3D NONLINEAR SIMULATIONS OF RBM





BASIC EQUATIONS

A. Zeiler, J. F. Drake and B. Rogers, Phys. Plasmas **4**, 2134, 1997

$$\frac{dn}{dt} + \frac{c_s^2}{\Omega_i L_n} \frac{\partial \phi}{\partial y} + \frac{2c_s^2}{\Omega_i} \vec{b} \times \vec{k} \cdot \nabla (\phi - n) - \nabla_{\parallel} J + c_s \nabla_{\parallel} v_{\parallel} = 0$$

$$\frac{c_s^2}{\Omega_i^2} \nabla_{\perp} \cdot \frac{d}{dt} \nabla_{\perp} \phi - \frac{2c_s^2}{\Omega_i} \vec{b} \times \vec{k} \cdot \nabla p_e - \nabla_{\parallel} J = 0$$

$$\frac{1}{v_A} \frac{\partial \psi}{\partial t} + \frac{c_s^2}{v_A \Omega_i L_p} \frac{\partial \psi}{\partial y} - \nabla_{\parallel} (\phi - n) = \frac{J}{\sigma}$$

$$\frac{dv_{\parallel}}{dt} = -c_s \left[\nabla_{\parallel} p_e + \frac{c_s^2}{v_A \Omega_i L_p} \frac{\partial \psi}{\partial y} \right]$$

$$J = v_A \frac{c_s^2}{\Omega_i^2} \nabla_{\perp}^2 \psi$$

$$\nabla_{\parallel} = \nabla_{\parallel 0} + \frac{c_s^2}{\Omega_i^2} \nabla_{\zeta} \times \nabla \psi \cdot \nabla$$

$$\frac{d}{dt} = \frac{\partial}{\partial t} + \frac{c_s^2 R_0}{\Omega_i^2} \nabla_{\zeta} \times \nabla \phi \cdot \nabla$$

$$n = \frac{\tilde{n}}{n_0}, \quad \phi = \frac{e\tilde{\phi}}{T_e}, \quad \sigma = \frac{T_e}{\eta_{\parallel} n_0 e^2}$$

$$v_{\parallel} = \frac{\tilde{v}_{\parallel}}{c_s}, \quad \psi = \frac{\Omega_i v_A}{c_s^2 B_0} \tilde{\psi}$$



BASIC EQUATIONS-CONTINUED

$$\frac{c_s^2}{\Omega_i^2} \nabla_{\perp} \cdot \frac{d}{dt} \nabla_{\perp} \phi - \frac{2c_s^2}{\Omega_i} \mathbf{b} \times \boldsymbol{\kappa} \cdot \nabla p_e - \nabla_{\parallel} J = 0$$

$$\mathbf{x}_{\perp} \rightarrow \mathbf{x}_{\perp}/L_0, \quad \mathbf{x}_{\parallel} \rightarrow \mathbf{x}_{\parallel}/L_{\parallel}, \quad t \rightarrow t/t_0 \quad L_{\parallel} = 2\pi qR, \quad n/t_0 \sim c_s^2 \phi / L_0 L_n \Omega_i, \quad J \sim \sigma \nabla_{\parallel} \phi$$

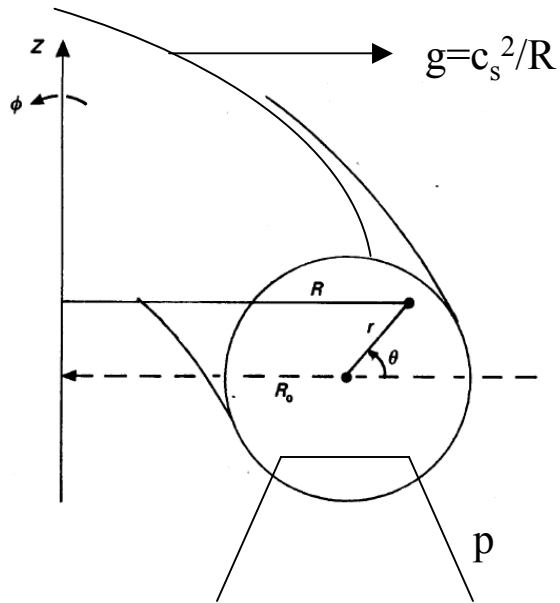
$$1 \quad : \quad \frac{RL_n}{2c_s^2} t_0^2 \quad : \quad \frac{4\pi v_A^2 \eta_{\parallel} t_0 L_0^2}{c^2 L_{\parallel}^2}$$

$$\Rightarrow t_0 = c_s \left(\frac{2}{RL_n} \right)^{1/2} \quad L_0 = \frac{L_{\parallel} c}{v_A} \left(\frac{\eta_{\parallel}}{4\pi t_0} \right)^{1/2}$$

Two dimensionless parameters: (1) $\alpha_D = \omega_* t_0$ (2) $\alpha_{\text{MHD}} = \left(\frac{v_A}{qR} t_0 \right)^2$



BALLOONING MODES



$$\omega^2 = -\frac{c_s^2}{RL_p} + k_{\parallel}^2 v_A^2$$

destabilization
RT-like mode

stabilization
Field-line
bending

$$k_{\parallel} = 1/qR$$

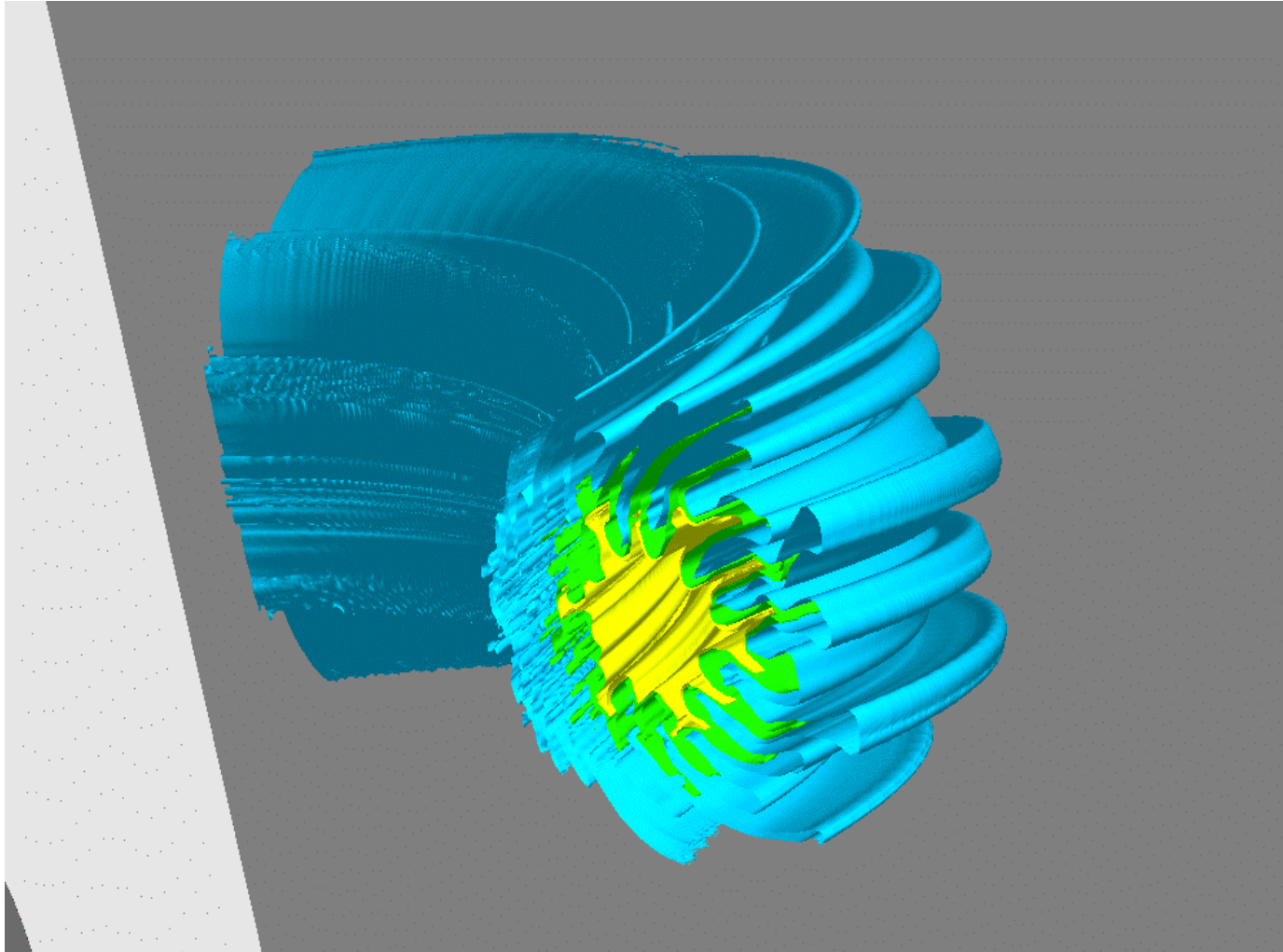
Instability Criterion for Ballooning Modes

$$\alpha = \frac{\beta q^2 R}{L_p} \sim 1$$



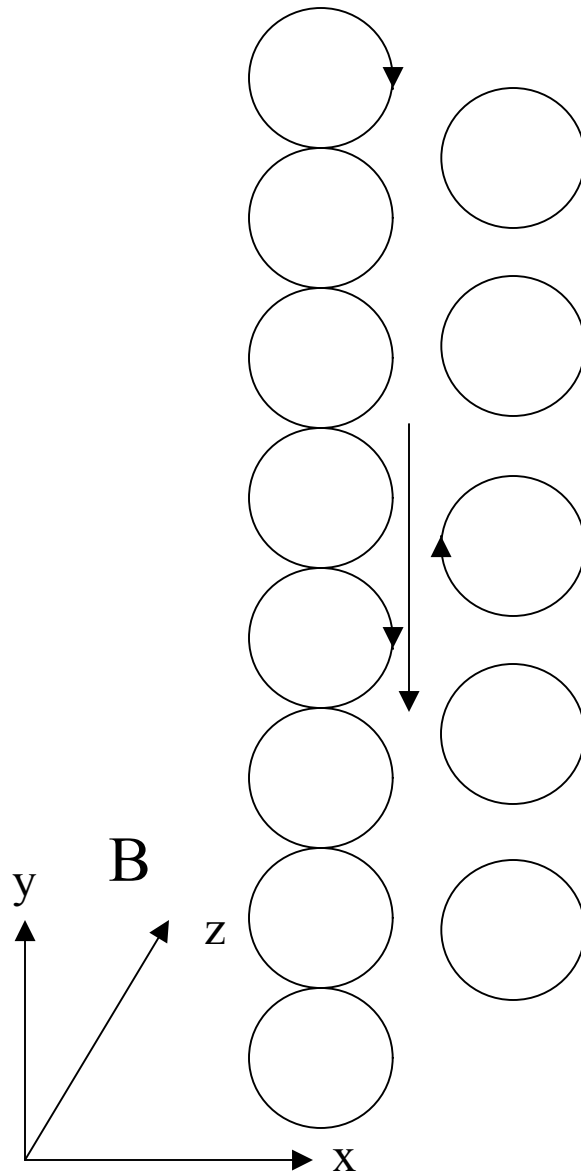
BALLOONING MODES 3D MHD SIMULATIONS KLEVA, GUZDAR PoP 8, 103, 2001

$$\eta = 3 \times 10^{-5}$$





DIAMAGNETIC CURRENTS AND DRIFTS



$$-\frac{\nabla p_\alpha}{n} + \frac{e_\alpha}{c} \vec{v}_{D\alpha} \times \vec{B} = 0, \quad \alpha = i, e$$

diamagnetic drift velocity

$$\vec{v}_{D\alpha} = c \frac{\nabla p_\alpha \times \vec{B}}{e_\alpha n B^2}$$

$$\frac{\partial n}{\partial t} + \nabla \cdot \left(n c \frac{\vec{E} \times \vec{B}}{B^2} \right) = 0, \quad \text{Ion Equation}$$

$$n = n_0 \exp\left(\frac{e\phi}{T_e}\right) \quad \text{Electron Boltzmann Response}$$

Linearize equations in inhomogeneous plasma (in x)

$$\sim e^{-i\omega t + ik_y y}$$

$$\frac{\tilde{n}}{n_0} = \frac{k_y v_{de}}{\omega} \frac{e\tilde{\phi}}{T_e}, \quad v_{De} = -\frac{c T_e}{e B n_0} \frac{dn_0}{dx}$$

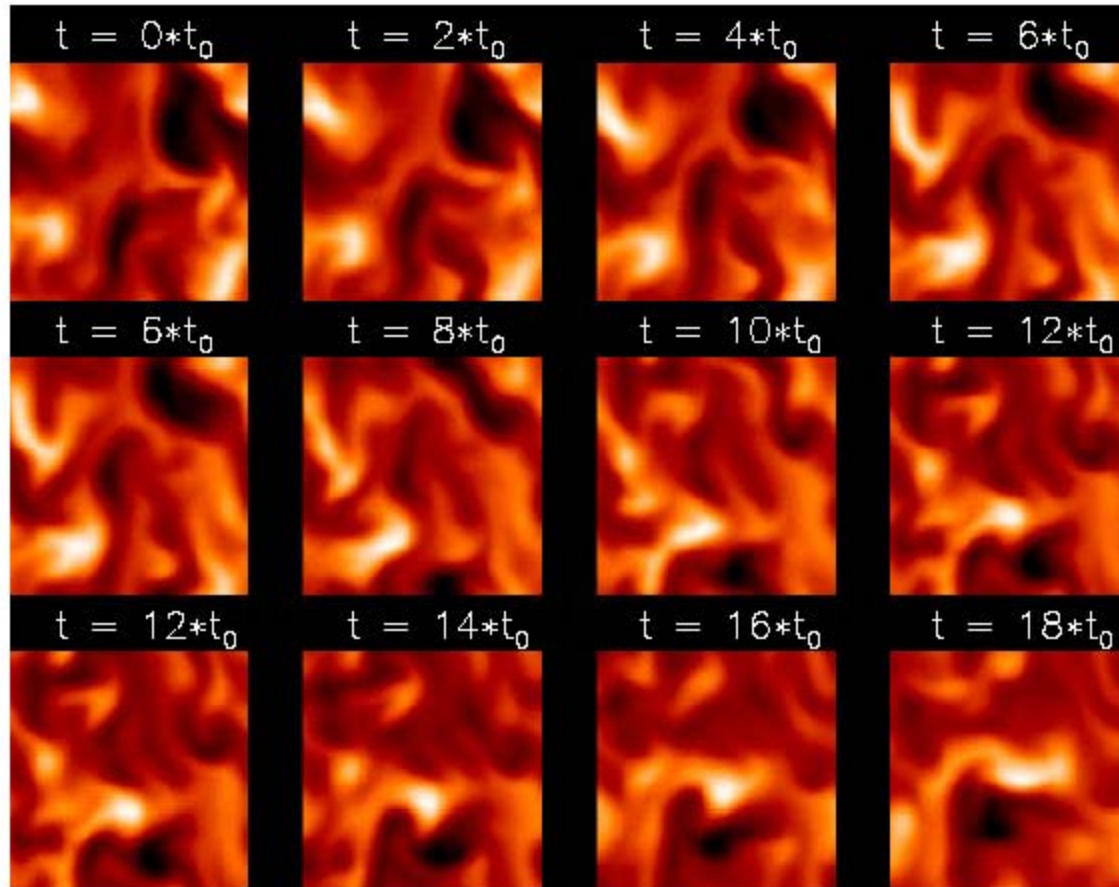
$$\frac{\tilde{n}}{n_0} = \frac{e\tilde{\phi}}{T_e}$$

$$\omega = k_y v_{De} \quad \text{drift wave}$$



Rogers, Drake and Zeiler, Simulations

Structure of fluctuations in the plane perpendicular to the magnetic field on outboard side



DBM code results for edge turbulence in C-Mod
6 cm radial x 6 cm poloidal x $\approx 1 \mu\text{sec}$ / frame



Rogers, Drake and Zeiler, PRL, 81, 4396, 1998

Simulations with evolving density profile

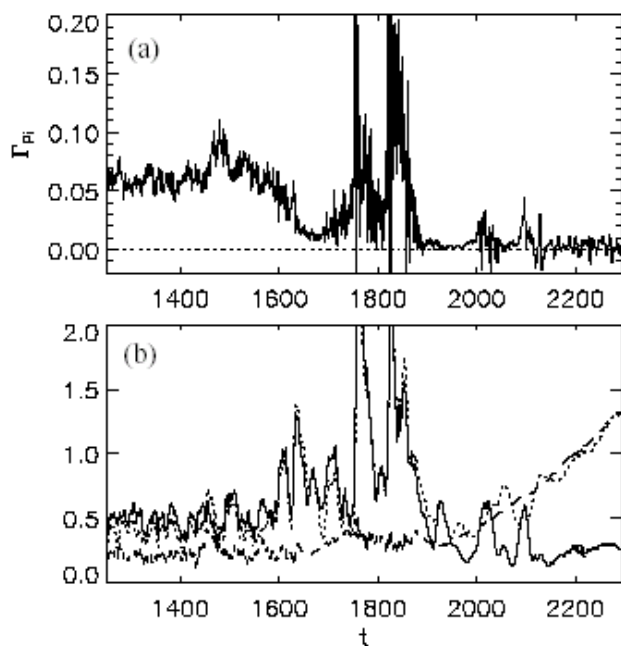


FIG. 4. (a) Γ_{pi} vs t ; (b) \bar{v}_{iy} (solid line); \bar{v}_{diy} (dashed line); \bar{v}_{Ey} (dotted line).

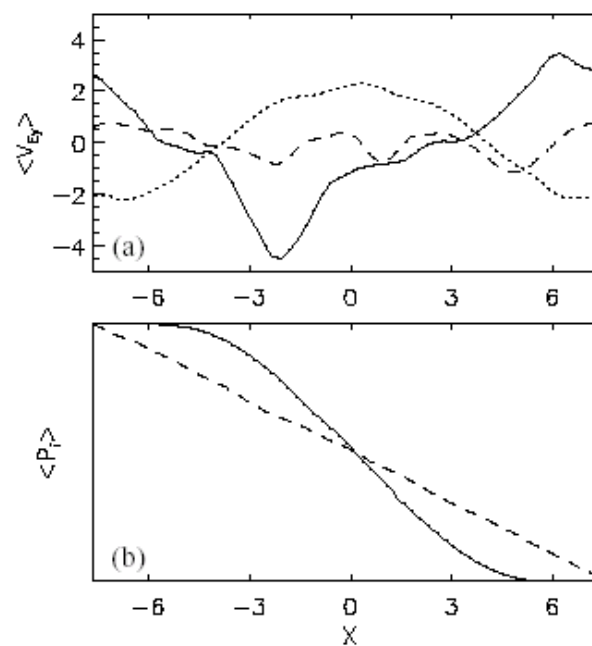
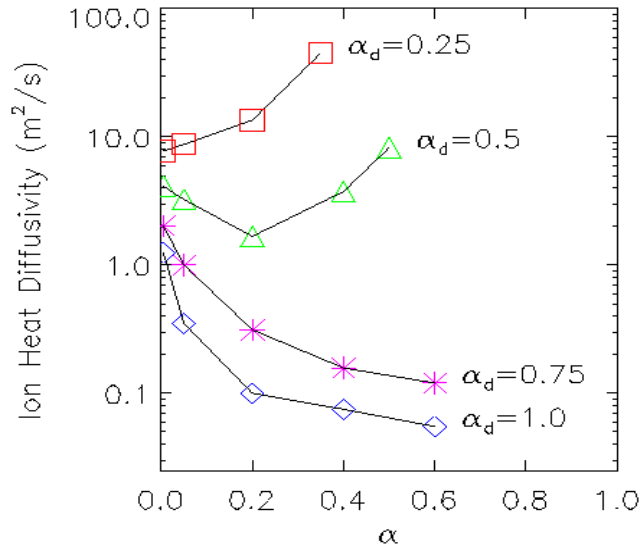


FIG. 5. (a) $\mathbf{E} \times \mathbf{B}$ flows before (dashed line), during (solid line), after (dotted line) transition; (b) early (dashed line), late (solid line) p_i profiles.

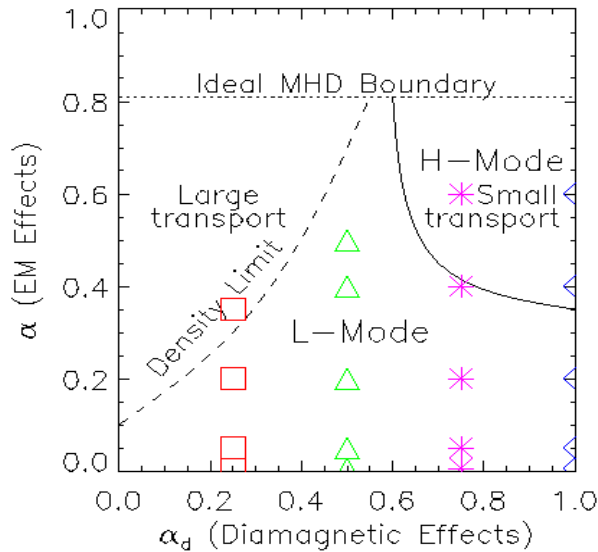


Rogers, Drake and Zeiler, PRL, 81, 4396, 1998



$$\alpha_D = \frac{\rho_s c_s t_0}{L_0 L_n (1 + \tau)}, \quad t_0 = \frac{(R L_n / 2)^{1/2}}{c_s}$$

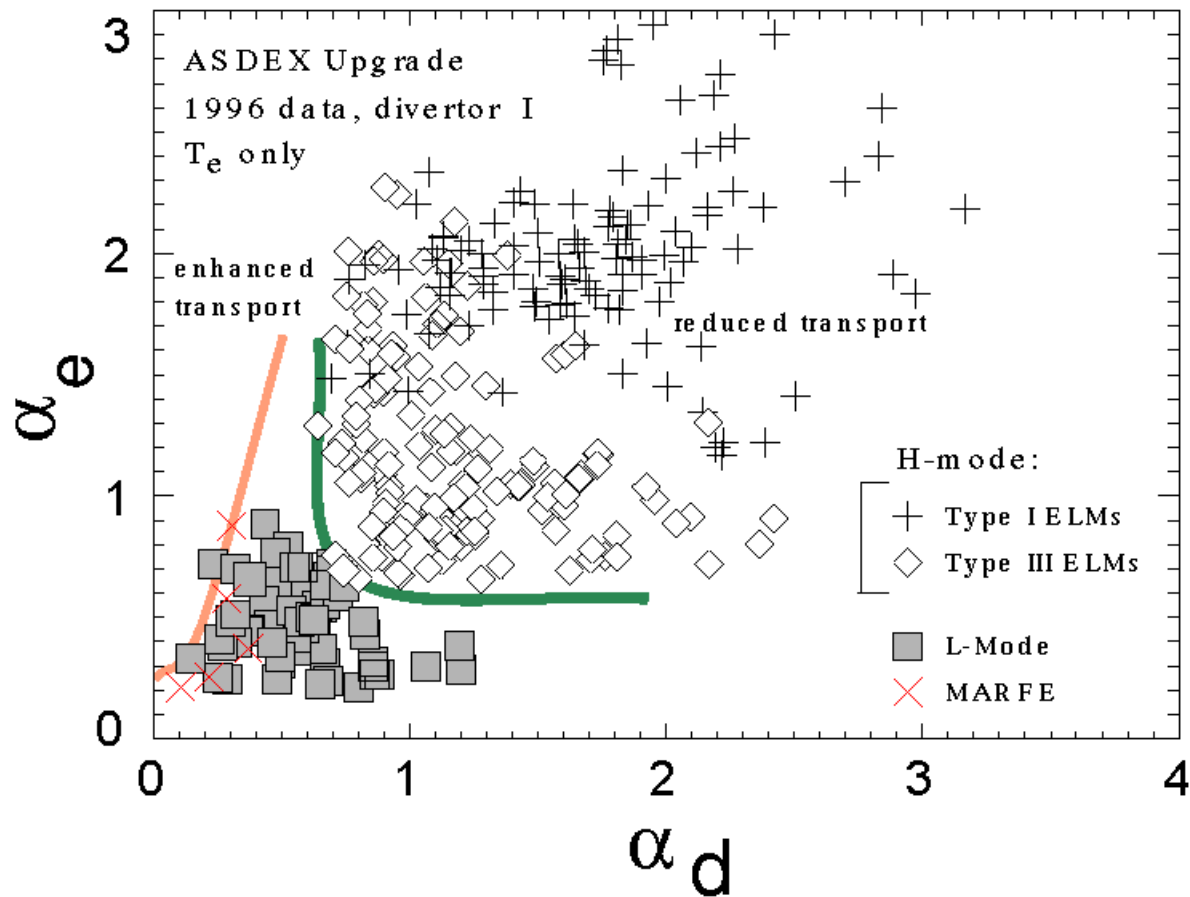
$$\alpha = \frac{q^2 R \beta}{L_p}, \quad \frac{L_n}{L_p} = \frac{[1 + \eta_e + \tau(1 + \eta_i)]}{(1 + \tau)}$$



$$\tau = \eta_e = \eta_i = 1$$



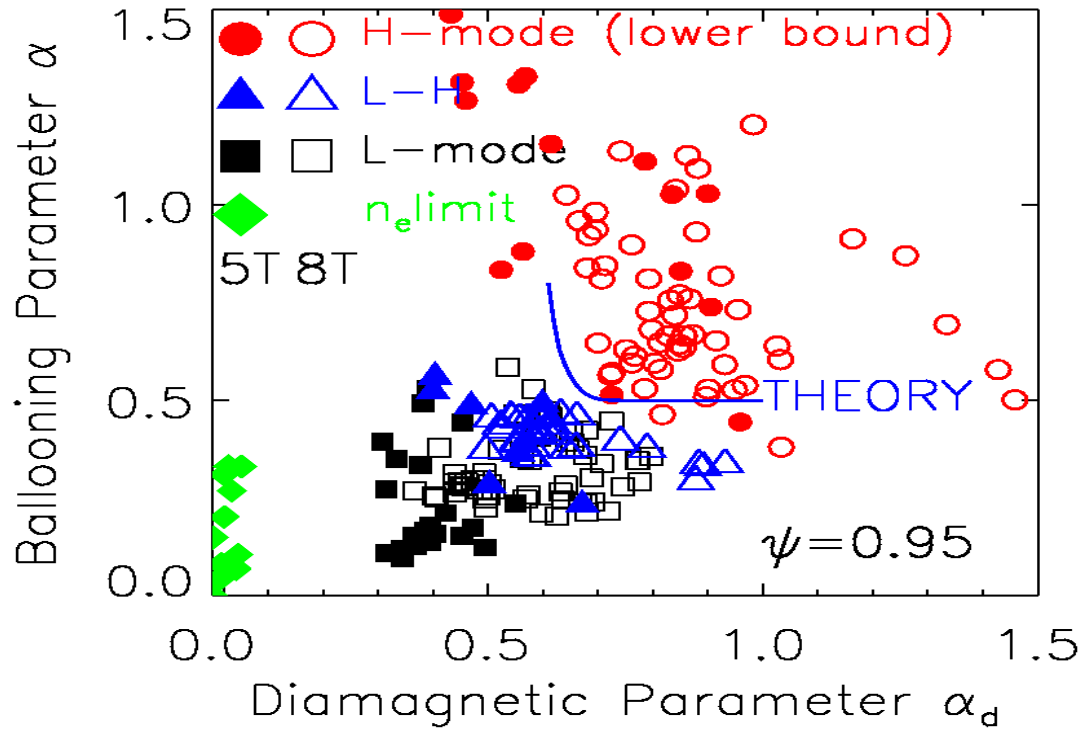
COMPARISON OF ASDEX RESULTS WITH CODE RESULTS





COMPARISON OF C-MOD RESULTS WITH CODE RESULTS

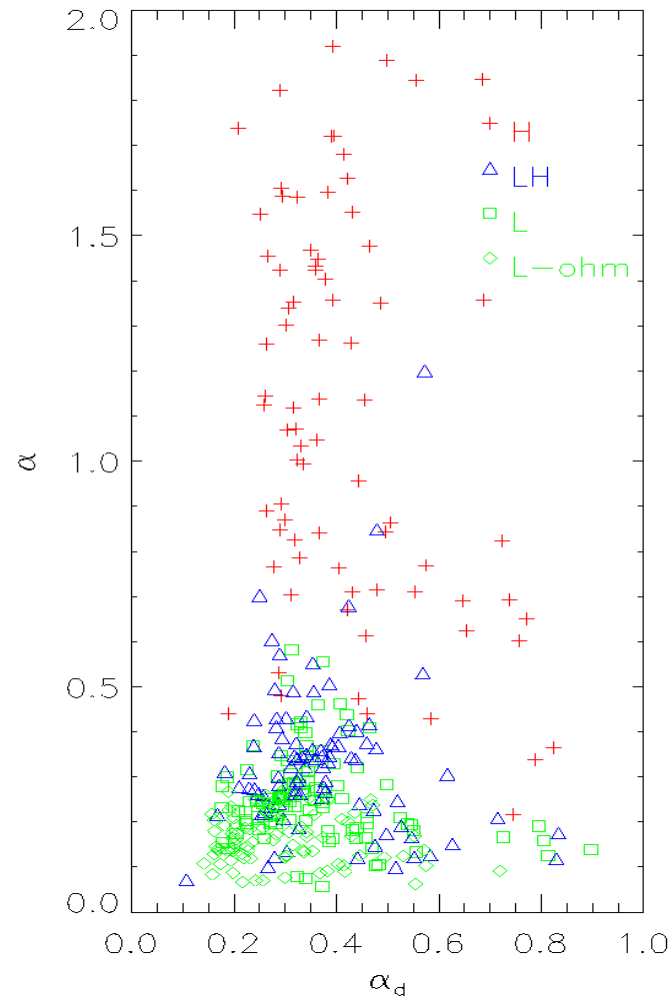
C-Mod (A. Hubbard)





D-IIID RESULTS WITH CODE RESULTS

DIIID (T. Carlstrom)





“HINTS” FROM 3D SIMULATIONS

→ “Transition” to improve confinement occurs for $\alpha_D \sim 1$,

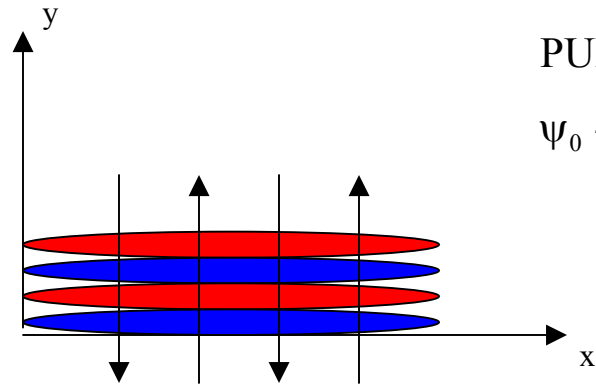
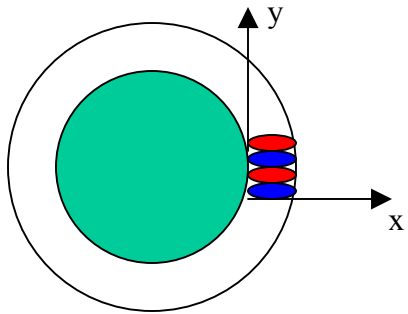
→ L-mode turbulence in the drift wave-like regime (not the resistive ballooning regime)

→ Increase in plasma β caused larger anomalous transport even for $\alpha_{\text{MHD}} < 1.0$
Rogers and Drake, Phys. Rev. Lett. **79**, 229 (1997)

→ Shear flow present in the L-mode phase
Shear flow necessary but not sufficient for L-H transitions

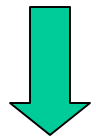


“MODULATION” INSTABILITY



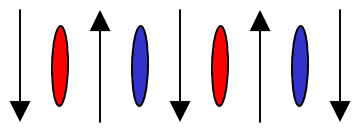
PUMP WAVE

$$\psi_0 \sim e^{-i\omega_0 t + ik_y y + ik_{\parallel} z}$$



ZONAL FLOW/FIELD

$$\tilde{\psi}_s \sim e^{-i\omega t + ik_x x}$$





LINEAR INSTABILITY ANALYSIS

Chen, Lin, White, Phys. Plasmas **7**, 3149, 2000, Guzdar et al., PRL, **86**, 15001, 2001.

$$\begin{aligned} \begin{Bmatrix} \phi \\ \psi \end{Bmatrix} &= e^{-i\omega t} \underbrace{\begin{Bmatrix} \phi_s \\ \psi_s \end{Bmatrix} e^{ik_x x}}_{\text{"shear" flow}} + \underbrace{e^{-i\omega_0 t} \begin{Bmatrix} \phi_0 \\ \psi_0 \\ n_0 \end{Bmatrix} e^{ik_y y + ik_{\parallel} z}}_{\text{pump wave}} \\ &+ \underbrace{e^{-i\omega_+ t} \begin{Bmatrix} \phi_+ \\ \psi_+ \\ n_+ \end{Bmatrix} e^{i(k_x x + k_y y + k_{\parallel} z)} + e^{-i\omega_- t} \begin{Bmatrix} \phi_- \\ \psi_- \\ n_- \end{Bmatrix} e^{i(k_x x - k_y y - k_{\parallel} z)}}_{\text{two side bands}} \end{aligned}$$

with $\omega_{\pm} = \omega \pm \omega_0$



“LOCAL” INSTABILITY ANALYSIS (1)

$$\nabla_{\parallel} \rightarrow ik_{\parallel} = i(m - nq) / Rq$$

$$(\omega + \Delta)\phi_{+} = i\Gamma_z \left[\phi_0 \phi_s M_A(k_x, k_y) + \frac{\omega_0}{k_{\parallel} v_A} \phi_0 \psi_s M_B(k_x, k_y) \right]$$

$$(\omega - \Delta)\phi_{-} = -i\Gamma_z \left[\phi_0^* \phi_s M_A(k_x, k_y) + \frac{\omega_0}{k_{\parallel} v_A} \phi_0^* \psi_s M_B(k_x, k_y) \right]$$

$$(\omega + iv_{\phi})\phi_s = i\Gamma_z \left[1 - \left(\frac{\omega_0}{k_{\parallel} v_A} \right)^2 \right] [\phi_0^* \phi_{+} - \phi_0 \phi_{-}]$$

$$(\omega + iv_{\psi})\psi_s = i\Gamma_z (k_x^2 \rho_s^2) \frac{\omega_0}{k_{\parallel} v_A} [\phi_0^* \phi_{+} - \phi_0 \phi_{-}]$$



“LOCAL” INSTABILITY ANALYSIS (2)

$$M_A = \frac{(1 + \tau)(1 + k_y^2 \rho_s^2 \tau)}{\left(1 + \frac{\omega_{*e}}{\omega_0} \tau\right) A} - \frac{\omega_0^2}{k_{\parallel}^2 v_A^2 A} \left[\frac{1 + k_{\perp}^2 \rho_s^2 \tau}{1 + k_y^2 \rho_s^2 \tau} \left(1 + \frac{\omega_{*e}}{\omega_0} \tau\right) + (1 + \tau) \left(1 - \frac{\omega_{*e}}{\omega_0}\right) \right] +$$

$$\left[\frac{\omega_0^2}{k_{\parallel}^2 v_A^2} \left(1 - \frac{\omega_{*e}}{\omega_0}\right) - k_{\perp}^2 \rho_s^2 \right] \left[\frac{k_x^2 - k_y^2}{k_{\perp}^2} - \tau \frac{k_y^2}{k_{\perp}^2} \frac{\left(\frac{\omega_{*e}}{\omega_0} - k_y^2 \rho_s^2\right)}{1 + k_y^2 \rho_s^2 \tau} \right] / A$$

$$M_B = \left[-\frac{2k_y^2}{k_{\perp}^2} \frac{1 + k_{\perp}^2 \rho_s^2 \tau}{1 + k_y^2 \rho_s^2 \tau} \left(1 - \frac{\omega_{*e}}{\omega_0} + k_y^2 \rho_s^2\right) \right] / A$$

$$\Gamma_z = \frac{k_x k_y c_s^2}{\Omega_i} \quad \Delta = k_x^2 \rho_s^2 \omega_0 (1 + \tau) / A$$



“LOCAL” INSTABILITY ANALYSIS (3)

$$A = 1 + k_{\perp}^2 \rho_s^2 (1 + \tau) - 3 \frac{\left\{ \omega_0 \left[\omega_0 + \frac{2}{3} \omega_{*e} (\tau - 1) \right] - \frac{1}{3} \omega_{*e}^2 \tau \right\}}{k_{\parallel}^2 v_A^2}$$

ω_0 is given by the dispersion relation

$$1 + k_y^2 \rho_s^2 (1 + \tau) - \frac{\omega_*}{\omega_0} - \frac{(\omega_0 - \omega_*)(\omega_0 + \omega_* \tau)}{k_{\parallel}^2 v_A^2} = 0$$

This dispersion relation has three roots, two Alfvén waves with effects of diamagnetic drifts and one drift wave with finite beta effects



“LOCAL” INSTABILITY ANALYSIS (4)

Finite T_i generalization of Guzdar, Kleva, Das and Kaw,
PRL, **86**, 15001, (2001) Dispersion Relation for the
Zonal Flow/Field Instability

$$\omega^2 - \Delta^2 + 2\gamma_z^2 M_A \left(1 - \frac{\omega_0^2}{k_{\parallel}^2 v_A^2}\right) + 2\gamma_z^2 M_B \frac{\omega_0^2}{k_{\parallel}^2 v_A^2} (k_x \rho_s)^2 = 0$$

$$\Delta = \frac{k_x^2 \rho_s^2 \omega_0 (1 + \tau)}{A}, \quad \Gamma_z = \frac{k_x k_y c_s^2}{\Omega_i}, \quad \gamma_z = \Gamma_z |\phi_0|$$



“LOCAL” INSTABILITY ANALYSIS (6)

Dispersion Relation solved numerically

1. Solve for the “pump” mode eigenfrequency for finite beta drift wave and drift-Alfven wave

$$\Omega_0 [1 + k_y^2 \rho_s^2 (1 + \tau)] - 1 - \Omega_0 k_y^2 \rho_s^2 \hat{\beta} (\Omega_0 - 1) (\Omega_0 + \tau) = 0$$

$$\text{where } \Omega_0 = \frac{\omega_0}{\omega_*} \quad \text{and} \quad \hat{\beta} = \beta \frac{q^2 R^2}{2L_n^2}$$

2. Use the eigenfrequency in dispersion relation for the shear flow/field to calculate growth rate

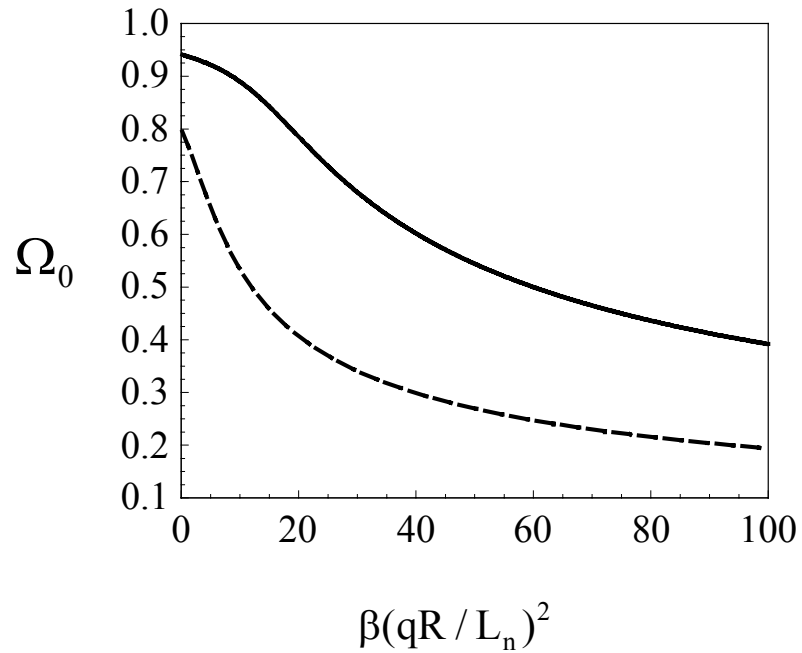
$$\hat{\gamma}_z = \left[\hat{M}_A (1 - k_y^2 \rho_s^2 \Omega_0^2 \hat{\beta}) + \hat{M}_B k_x^2 \rho_s^2 k_y^2 \rho_s^2 \Omega_0^2 \hat{\beta} - \hat{\Delta}^2 \right]^{1/2} \quad \hat{\Delta}^2 = \frac{1}{2} \left(\frac{\rho_s^2}{L_n^2} \right) \frac{(k_x^2 \rho_s^2)}{|\phi_0|^2}$$

Five dimensionless parameters :

$$(1) k_x \rho_s \quad (2) k_y \rho_s \quad (3) \hat{\beta} \quad (4) |\phi_0| L_n / \rho_s \quad (5) \tau = \frac{T_i}{T_e}$$



FINITE BETA DRIFT WAVE AS PUMP



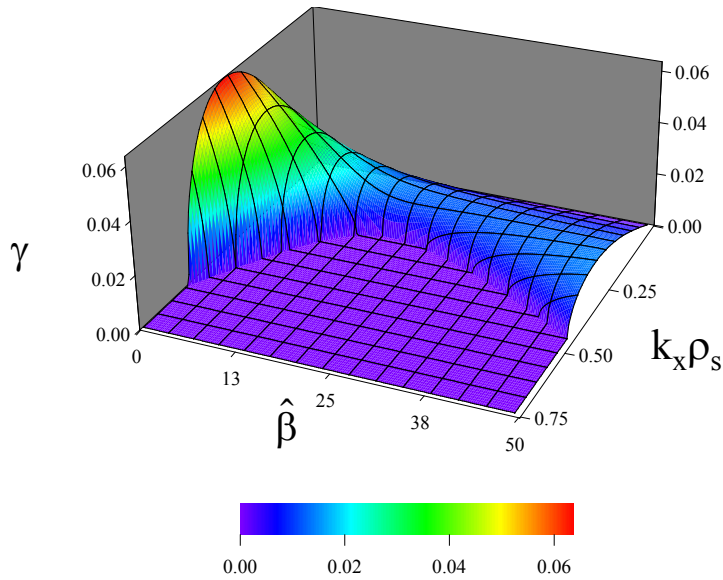
————— $k_y \rho_s = 0.25$

----- $k_y \rho_s = 0.50$

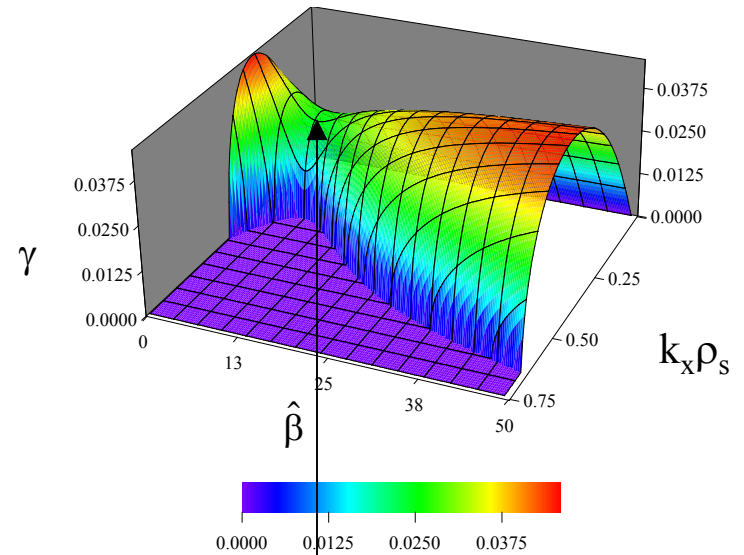


GROWTH RATE FOR ZONAL FLOW/FIELD

$$k_y \rho_s = 0.25, \quad e\phi/T_e = \rho_s/L_n$$



$\tau=0.0$



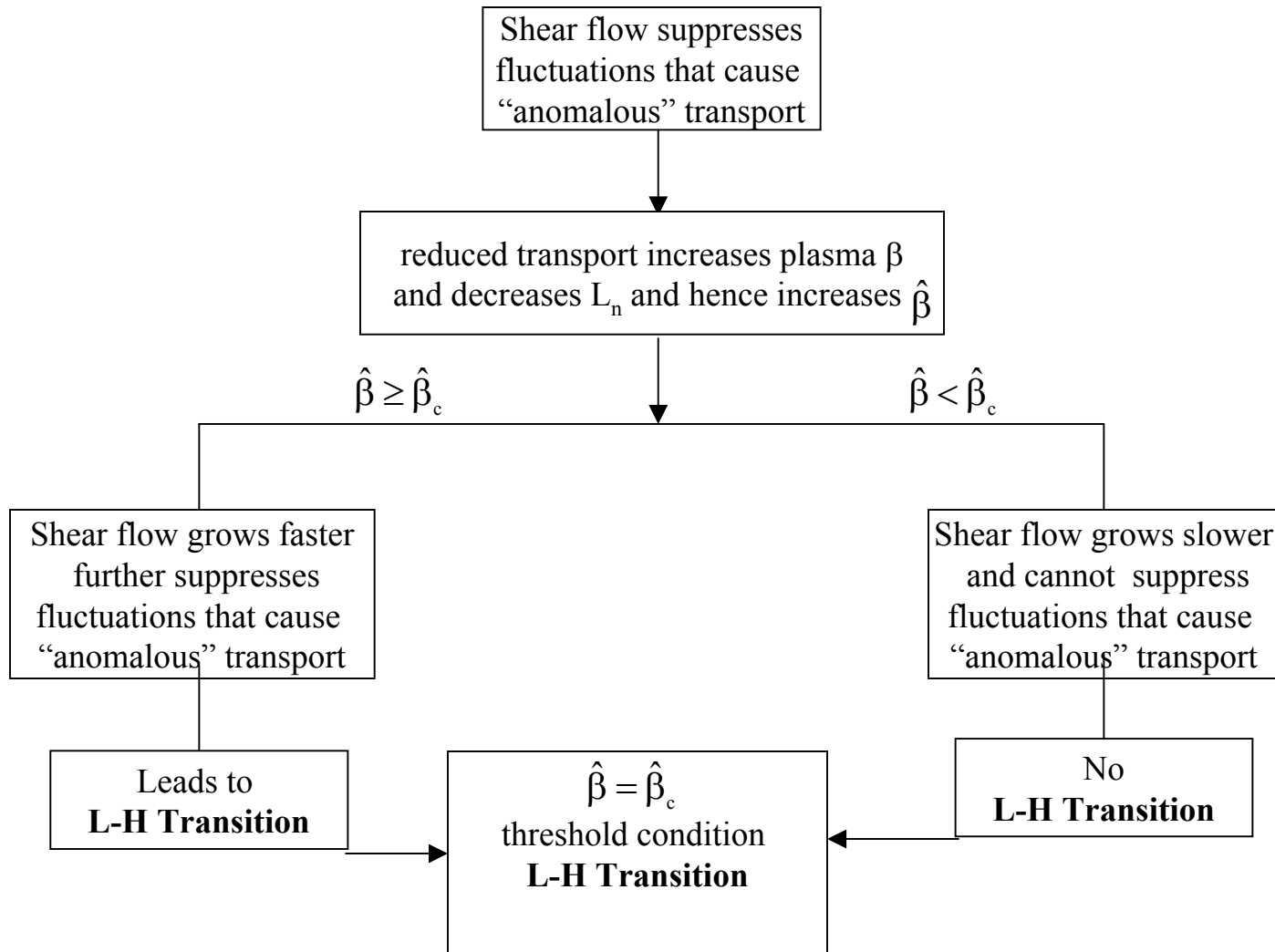
$\tau=1.0$

$\hat{\beta}_c$

THRESHOLD CONDITION FOR L-H TRANSITION
 MAXIMUM OF $(k_y \rho_s)^2 \hat{\beta}_c$ FOR $k_y \rho_s, \tau$ AND $e\phi/T_e$



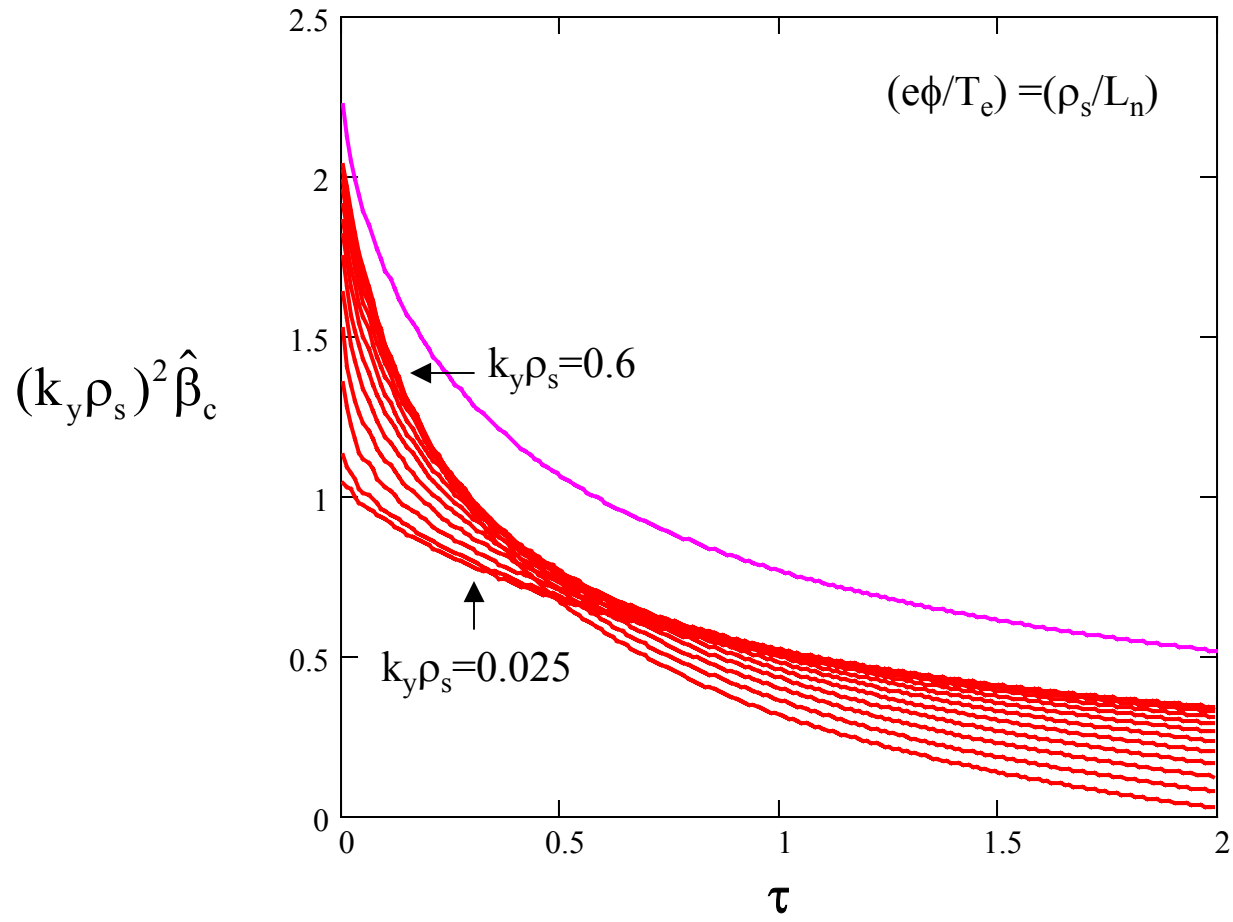
SCENARIO FOR L-H TRANSITION





$(k_y \rho_s)^2 \hat{\beta}_c$ vs τ

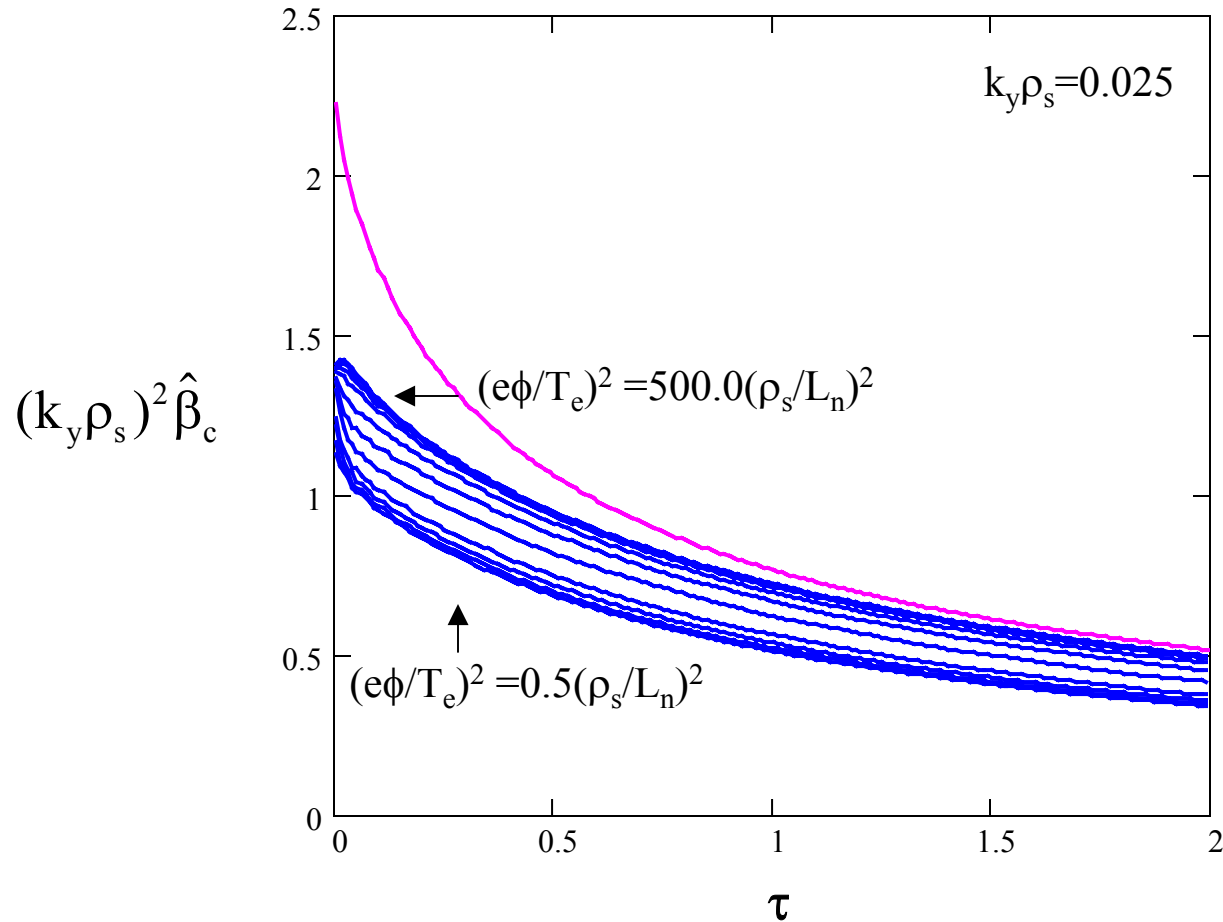
$k_y \rho_s = 0.025, 0.05, 0.1, 0.15, 0.2, 0.25, 0.3, 0.35, 0.4, 0.45, 0.5, 0.55, 0.6$





$(k_y \rho_s)^2 \hat{\beta}_c$ vs τ

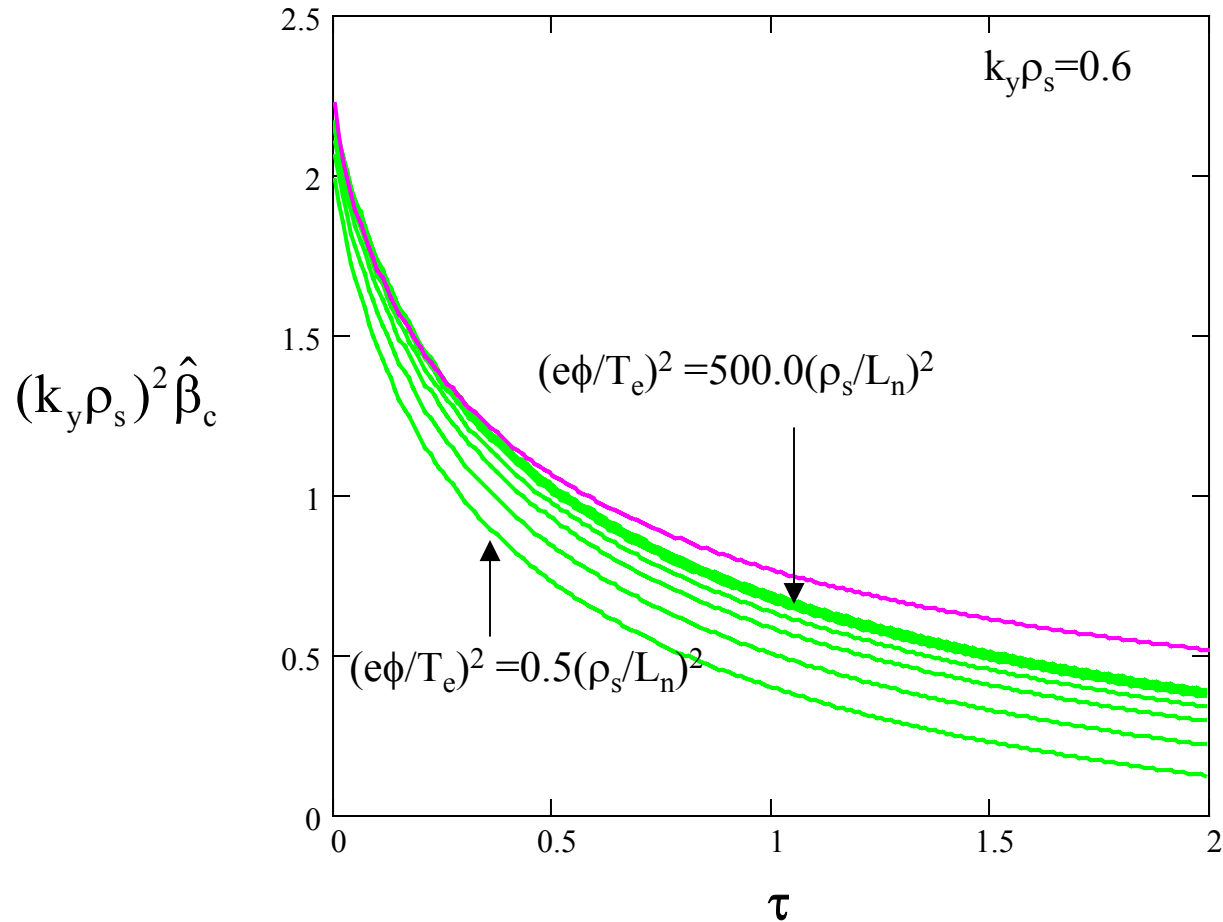
$$(e\phi/T_e)^2 = (500.0, 200.0, 100.0, 50.0, 20.0, 10.0, 5.0, 2.0, 1.0, 0.5)(\rho_s/L_n)^2$$



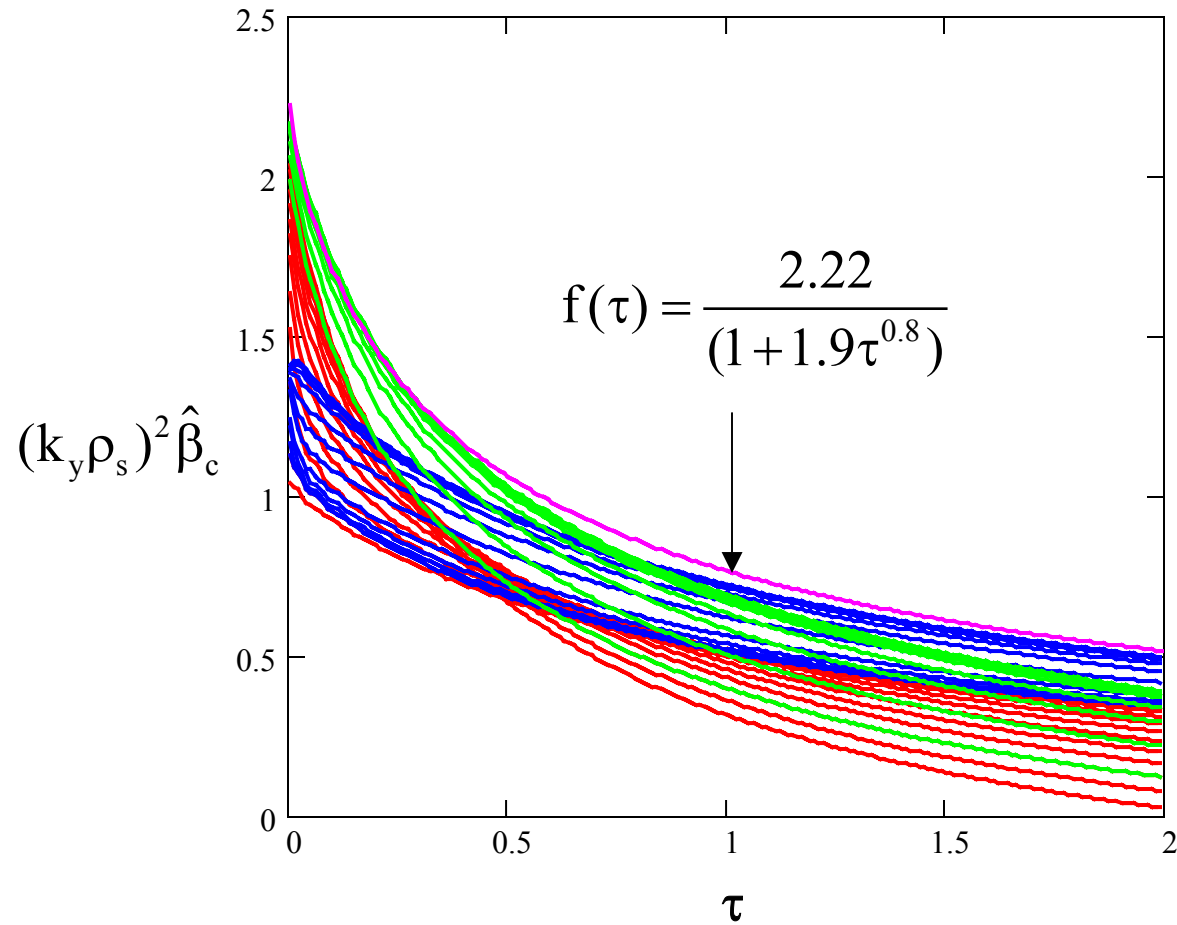


$(k_y \rho_s)^2 \hat{\beta}_c$ vs τ

$$(e\phi/T_e)^2 = (500.0, 200.0, 100.0, 50.0, 20.0, 10.0, 5.0, 2.0, 1.0, 0.5)(\rho_s/L_n)^2$$



$(k_y \rho_s)^2 \hat{\beta}_c$ vs τ





“COMPARISON” WITH CODE

Application of Finite Beta Drift Wave Case to Rogers-Drake-Zeiler Edge Simulations

From code, threshold curve for L-H Transition $\alpha_{\text{MHD}}\alpha_{\text{D}}^2=0.25$

$$k_y \sim 2\pi/L_0$$

Threshold Condition for Transition

$$\hat{\beta} = \hat{\beta}_c \text{ for } d\gamma/d\hat{\beta} = d^2\gamma/d\hat{\beta}^2 > 0$$

Reason: For $\beta > \beta_c$ transition to good confined state increases β , which increases growth of shear flow/field which further improves confinement.

$$(k_y \rho_s)^2 \hat{\beta}_c = 4\pi^2 (1 + \tau) \alpha_{\text{MHD}} \alpha_{\text{D}}^2 / [1 + \eta_e + \tau(1 + \eta_i)]$$

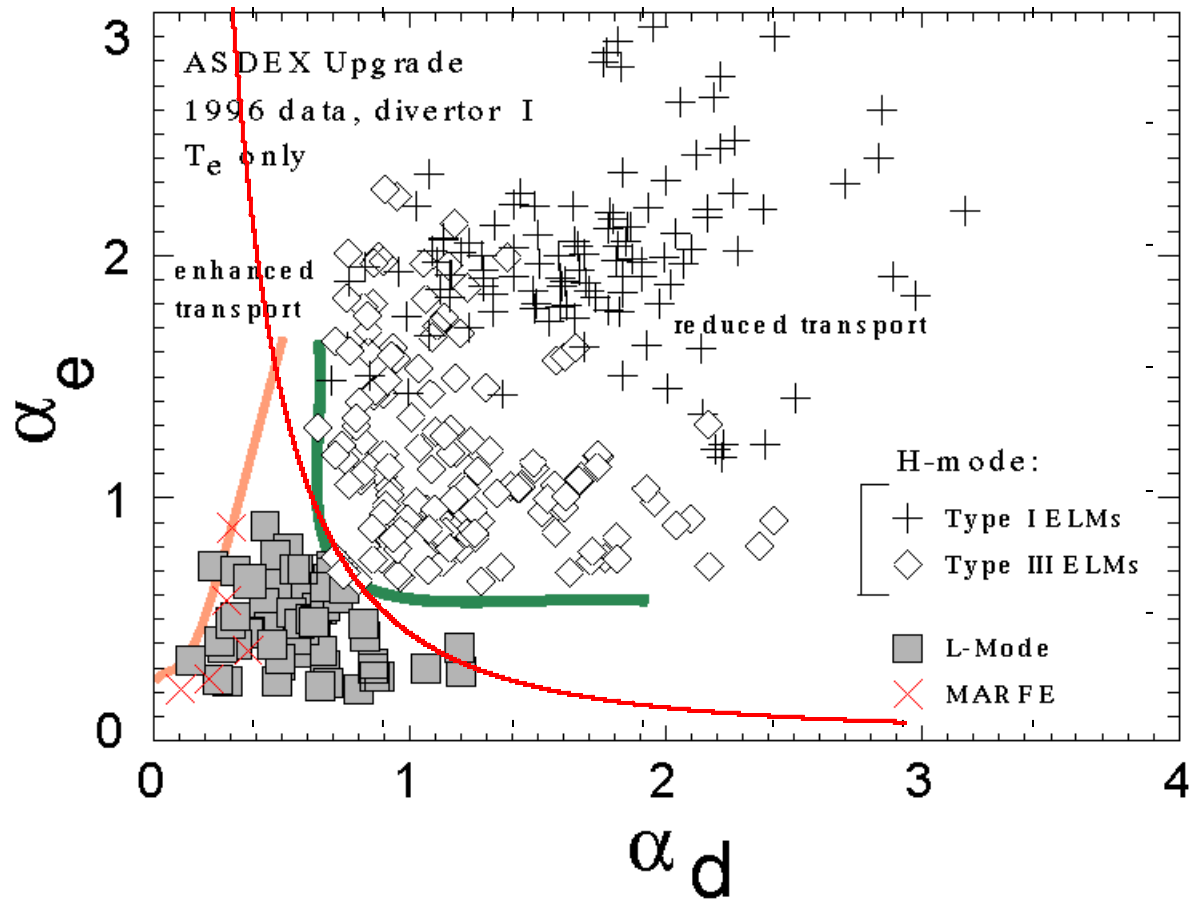
From our studies $(k_y \rho_s)^2 \beta_c = 1.7 - 2.15$

Hence from our theory

$$\alpha_{\text{MHD}} \alpha_{\text{D}}^2 = \mathbf{0.085 - 0.12}$$



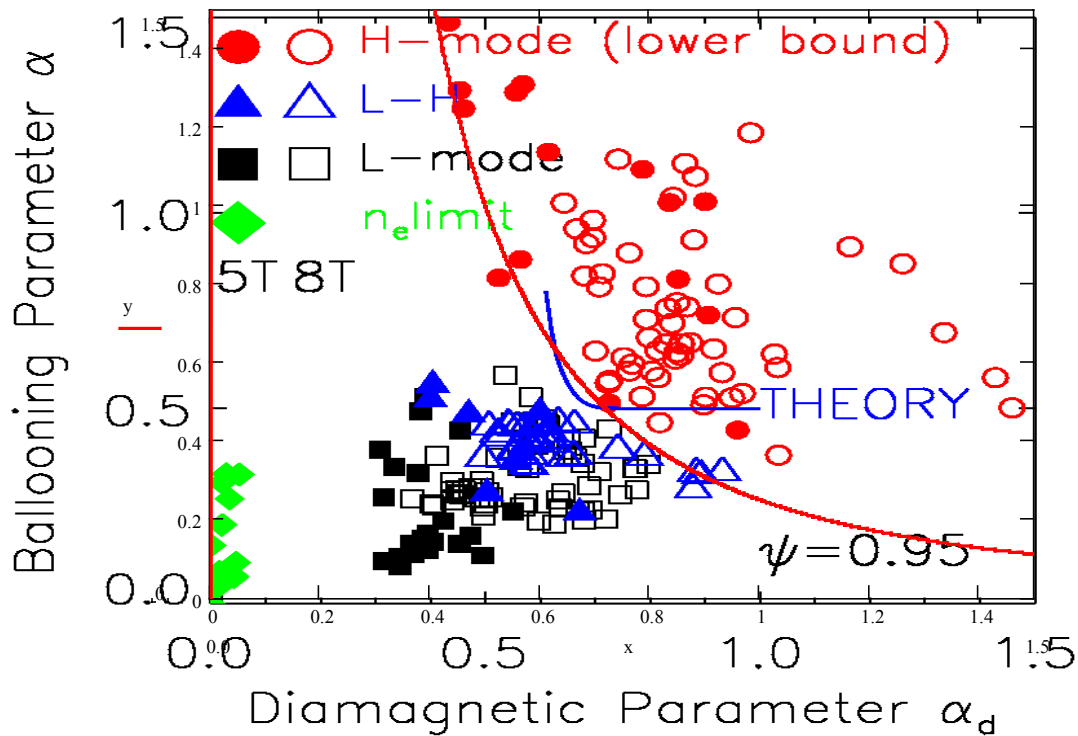
COMPARISON OF ASDEX RESULTS WITH CODE RESULTS





COMPARISON OF C-MOD RESULTS WITH CODE RESULTS

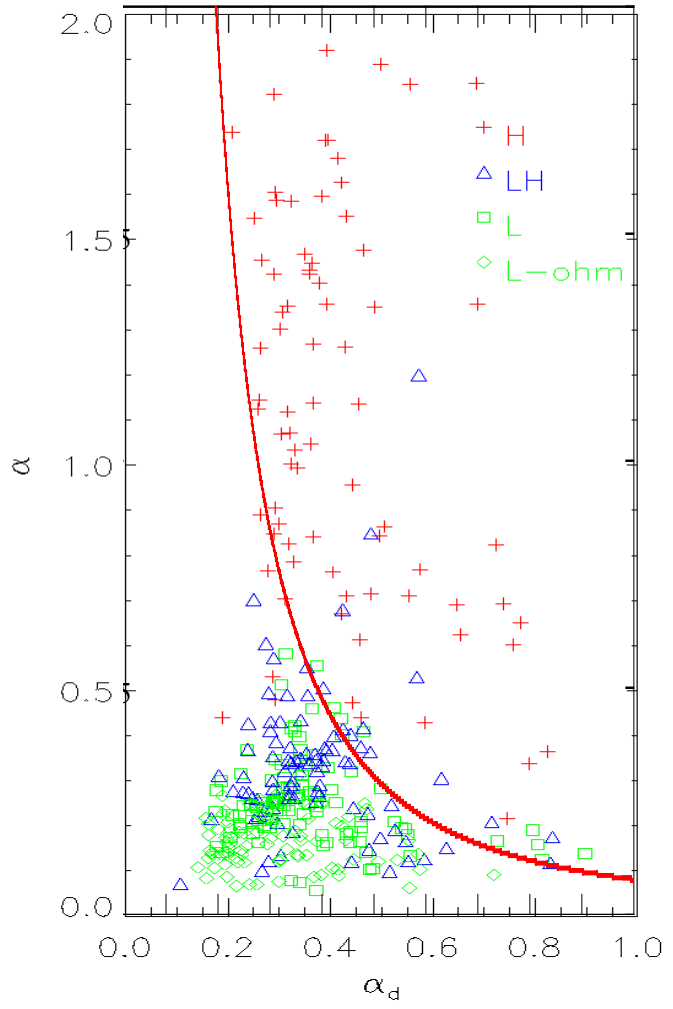
C-Mod (A. Hubbard)





D-IIID RESULTS WITH CODE RESULTS

DIIID (T. Carlstrom)





CRITICAL PARAMETER Λ OR CRITICAL T_e

$$k_y^2 \rho_s^2 \hat{\beta} = 2$$

$$k_y = 2\pi/L_0, \quad L_0 = 2\pi q \left(\frac{v_{ei} R \rho_s}{2\Omega_e} \right)^{1/2} \left(\frac{2R}{L_n} \right)^{1/4}$$

$$\frac{\rho_s^2}{L_0^2} \left(\frac{4\pi n T_e}{B^2} \right) \frac{q^2 R^2}{L_n^2} = \frac{1}{2\pi^2}$$

$$T_{ec} \text{ (keV)} = 0.45 (B^2 \text{ (T)} Z_{\text{eff}})^{1/3} \left(\frac{1}{R \text{ (m)} A_i} \right)^{1/6} L_n^{1/2} \text{ (m)}$$

OR

$$\Lambda = \frac{T_e \text{ (keV)} (R \text{ (m)} A_i)^{1/6}}{(B^2 \text{ (T)} Z_{\text{eff}})^{1/3} L_n^{1/2} \text{ (m)}}, \quad \text{with } \Lambda_c = 0.45$$



CRITICAL PARAMETER Λ OR CRITICAL T_e

$$k_y^2 \rho_s^2 \hat{\beta} = 2.22 / (1 + 1.9\tau^{0.8})$$

$$k_y = 2\pi / L_0, \quad L_0 = 2\pi q \left(\frac{v_{ei} R \rho_s}{2\Omega_e} \right)^{1/2} \left(\frac{2R}{L_n} \right)^{1/4}$$

$$\frac{\rho_s^2}{L_0^2} \left(\frac{4\pi n T_e}{B^2} \right) \frac{q^2 R^2 (1 + 1.9\tau^{0.8})}{L_n^2} = \frac{1.11}{2\pi^2}$$

$$T_{ec} \text{ (keV)} = 0.46 \left(\frac{B^2 \text{ (T)} Z_{\text{eff}}}{1 + 1.9\tau^{0.8}} \right)^{1/3} \left(\frac{1}{R \text{ (m)} A_i} \right)^{1/6} L_n^{1/2} \text{ (m)}$$

OR

$$\Lambda = \frac{T_e \text{ (keV)} (R \text{ (m)} A_i)^{1/6} (1 + 1.9\tau^{0.8})^{1/3}}{(B^2 \text{ (T)} Z_{\text{eff}})^{1/3} L_n^{1/2} \text{ (m)}}, \quad \text{with } \Lambda_c = 0.46$$



DATA FROM DIII-D

R. GROEBNER AND P. GOHIL

SHOT SERIES	:078151, 078153, 078155, 078156	I_p scan (1.0-2.0 MA) $B_T=2.1$ T, $n_e=4.0 \times 10^{19}/m^3$
	078161, 078165, 078167, 078169	B_T scan (1.1-2.1 T) $I_p=1.0$ MA, $n_e=4.0 \times 10^{19}/m^3$
	084026, 084032, 084040, 084044	n_e scan (1.4×10^{19} - $3.9 \times 10^{19}/m^3$) $I_p=1.3$ MA, $B_T=2.1$ T
	08830, 089348	Random selection $B_T=2.1$ T $I_p=1.0$ MA
	102014, 102015, 102016, 102017 102025, 102026, 102029	
SHOTS	96338, 96348	different ∇B drift $I_p=0.97$ MA, $B_T=2.1$ T
	99559, 100162	

Data T_e and L_n back-averaged over three points

To remove fluctuations from “turbulence”



CARLSTROM ET. AL, NUCLEAR FUSION 39, 1941, (1999)

Tanh fit of profiles

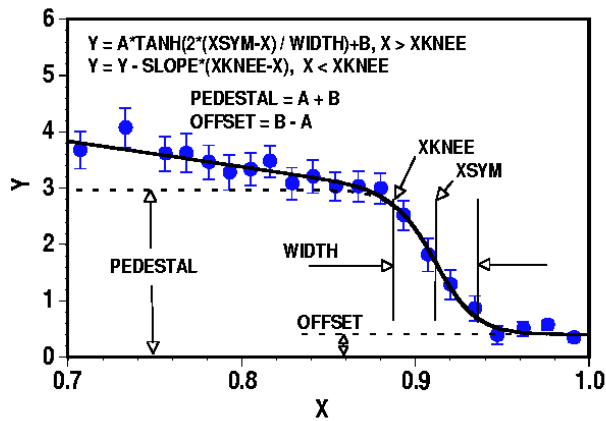


FIG. 3. Modified hyperbolic tangent fit to a typical L-mode edge n_e profile showing the location of the symmetry point, x_{sym} , and the profile knee, x_{knee} .

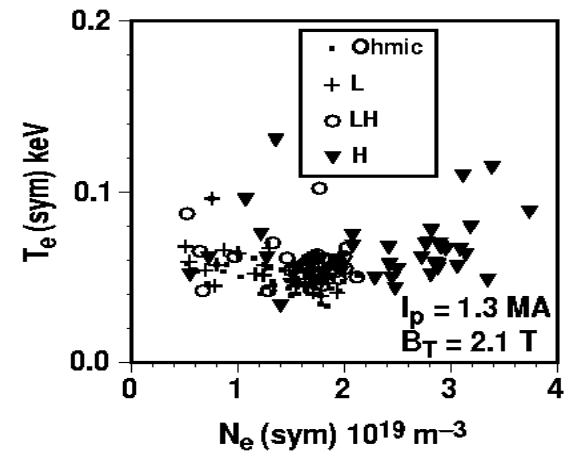
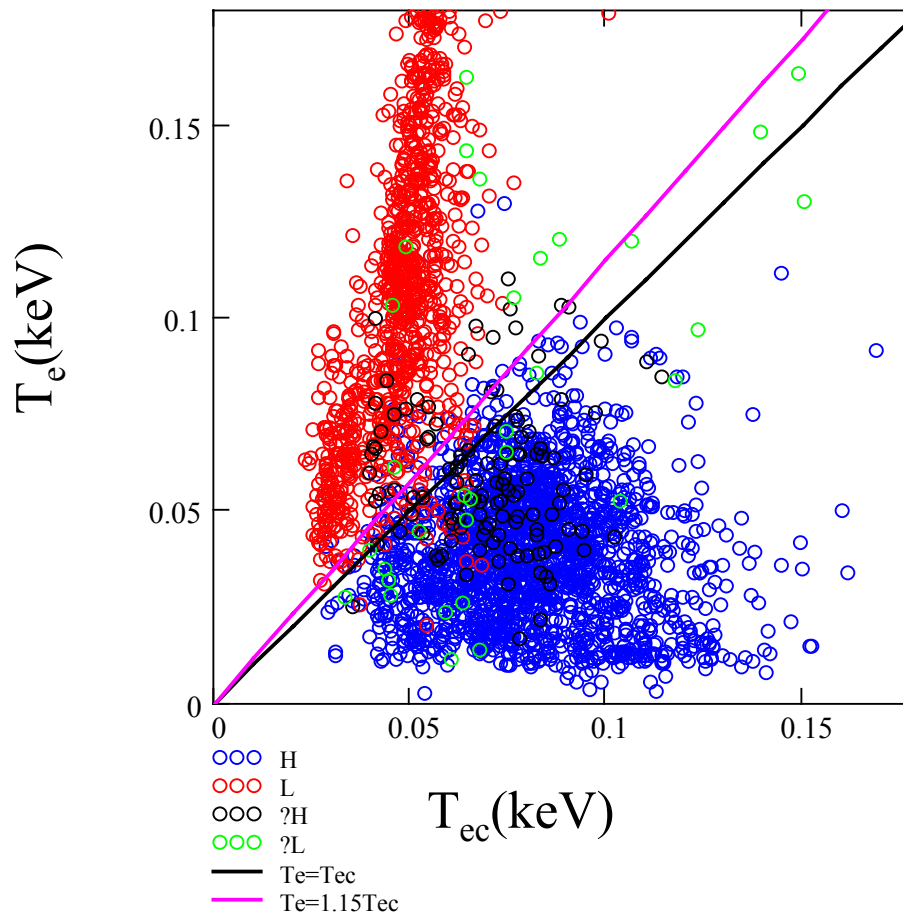


FIG. 6. Operational space diagram for the edge T_e and n_e evaluated at the n_e symmetry point.



COMPARISON WITH DIII-D (IN COLLABORATION WITH R. GROEBNER)--2

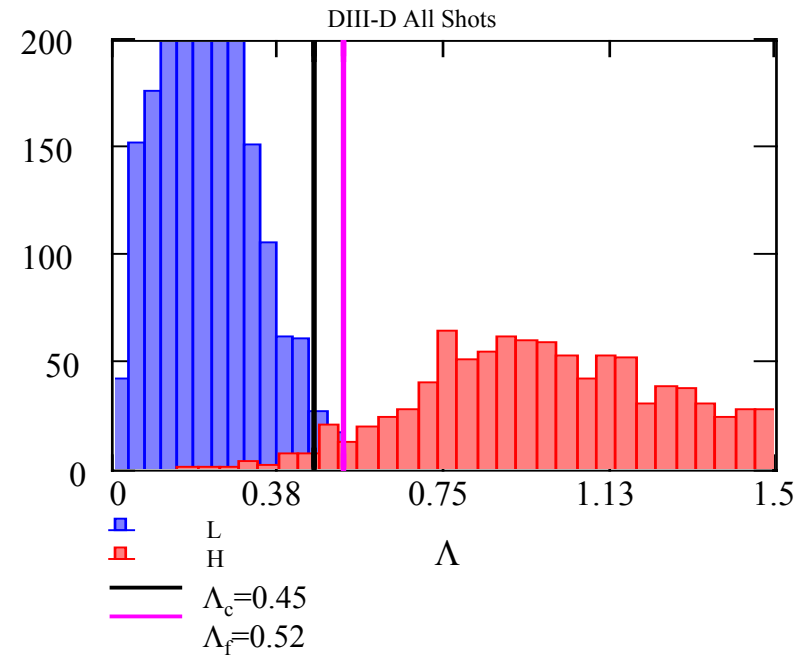
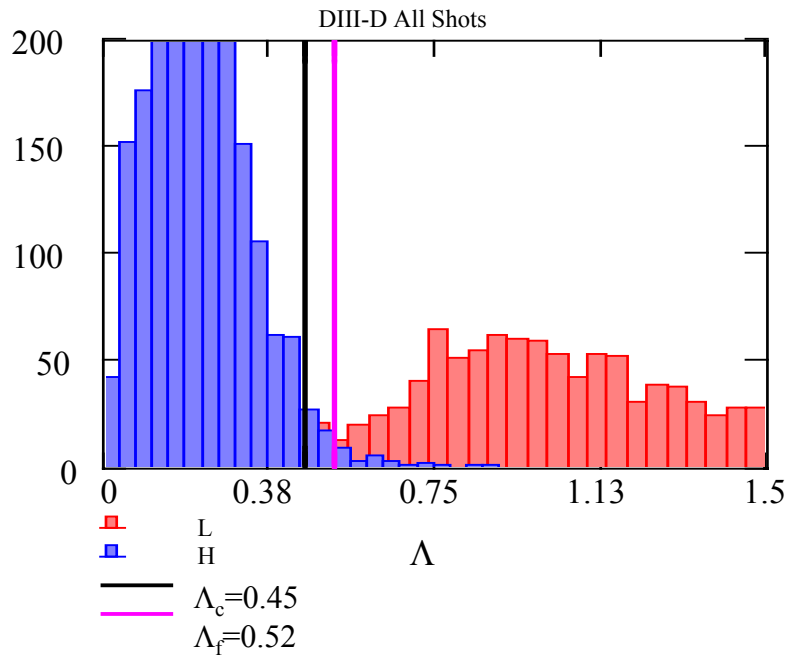
$$T_{ec}(\text{keV}) = 0.45 \frac{[B_T(\text{T})]^{2/3} [L_n(\text{m})]^{1/2} Z_{\text{eff}}^{1/3}}{[R(\text{m})A_i]^{1/6}}$$





COMPARISON WITH DIII-D

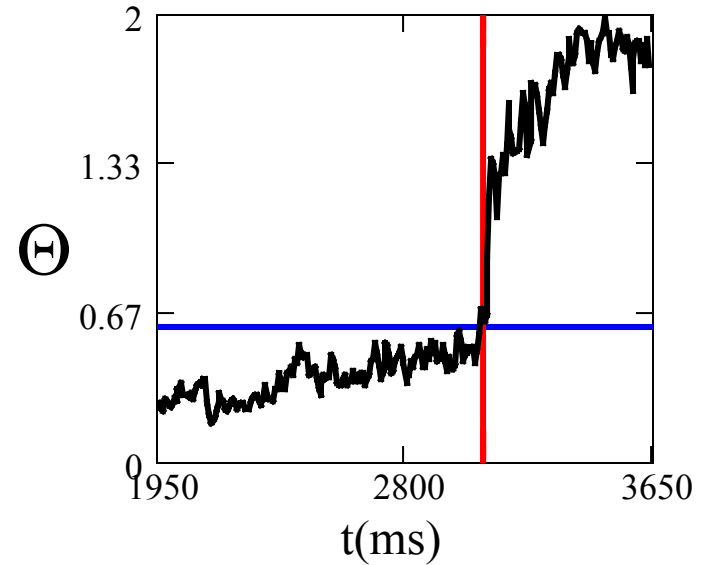
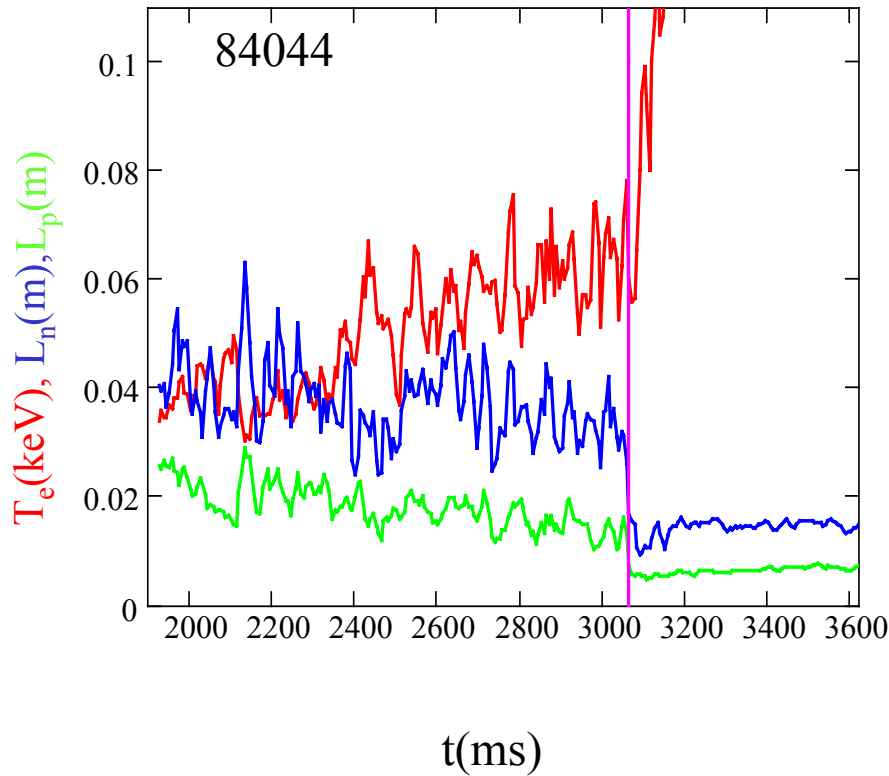
$$\Lambda = \frac{T_e(\text{keV})(R(\text{m})A_i)^{1/6}}{[B_T(\text{T})]^{2/3} [L_n(\text{m})]^{1/2} Z_{\text{eff}}^{1/3}}$$





COMPARISON WITH DIII-D

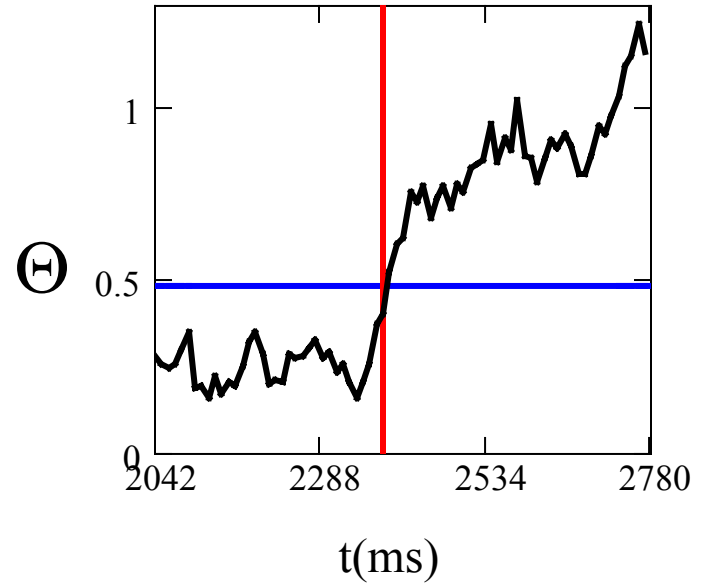
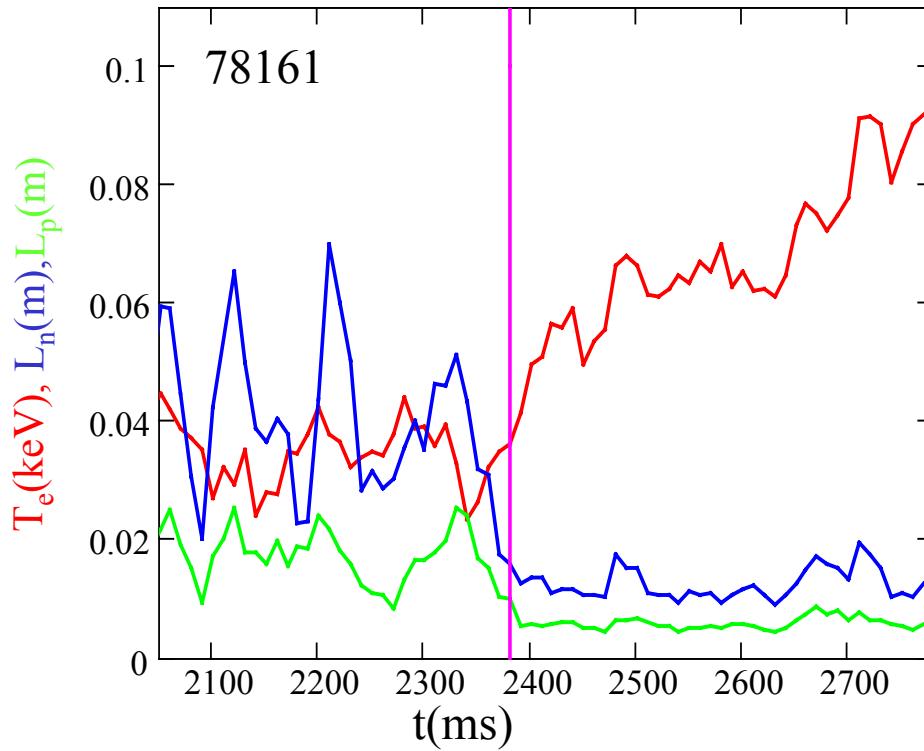
$B_T=2.11\text{T}$, $I_p=1.33\text{ MA}$, $\langle n \rangle=3.7 \times 10^{19}\text{ m}^{-3}$, ∇B towards X point





COMPARISON WITH DIII-D

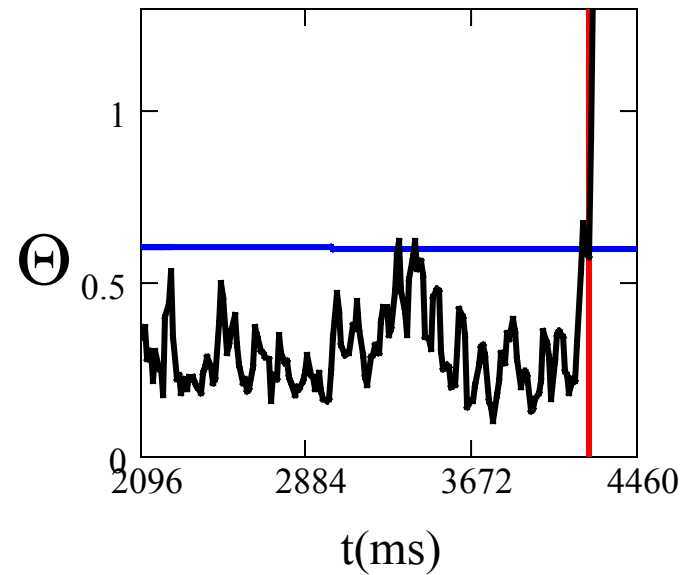
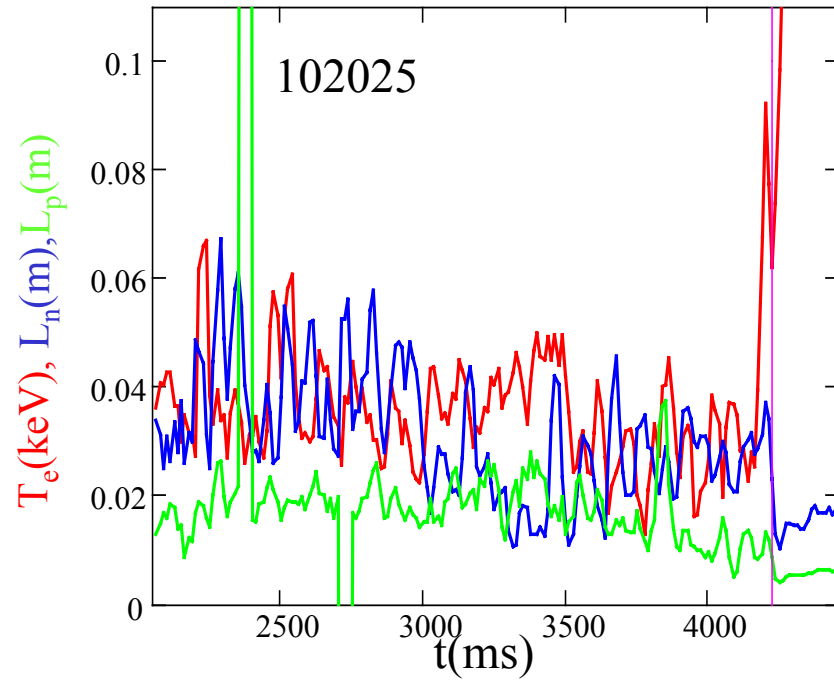
$B_T=1.51T$, $I_p=1.00$ MA, $\langle n \rangle=3.7 \times 10^{19} \text{ m}^{-3}$, ∇B towards X point



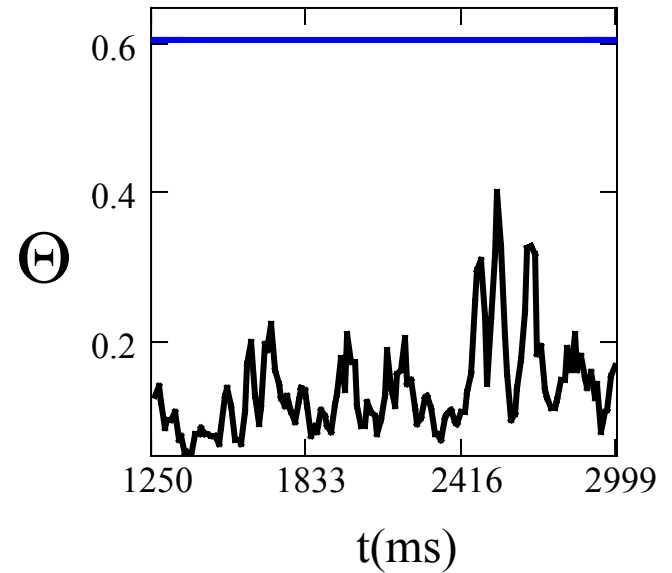
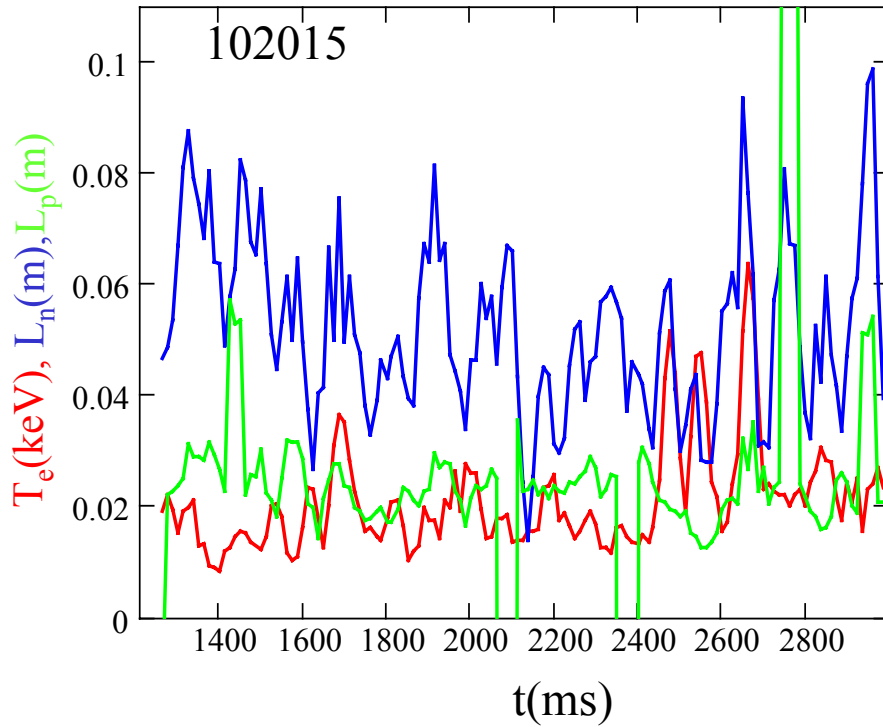


COMPARISON WITH DIII-D

$B_T=2.07T$, $I_p=1.57$ MA, $\langle n \rangle=4.7 \times 10^{19} \text{ m}^{-3}$,
 ∇B towards X point till $t=3450$ ms, changed to away



$B_T=2.12T$, $I_p=1.08$ MA, $\langle n \rangle=2.5-3.6 \times 10^{19} \text{ m}^{-3}$, ∇B away X point
Late time pellet injection, NO H-MODE!!





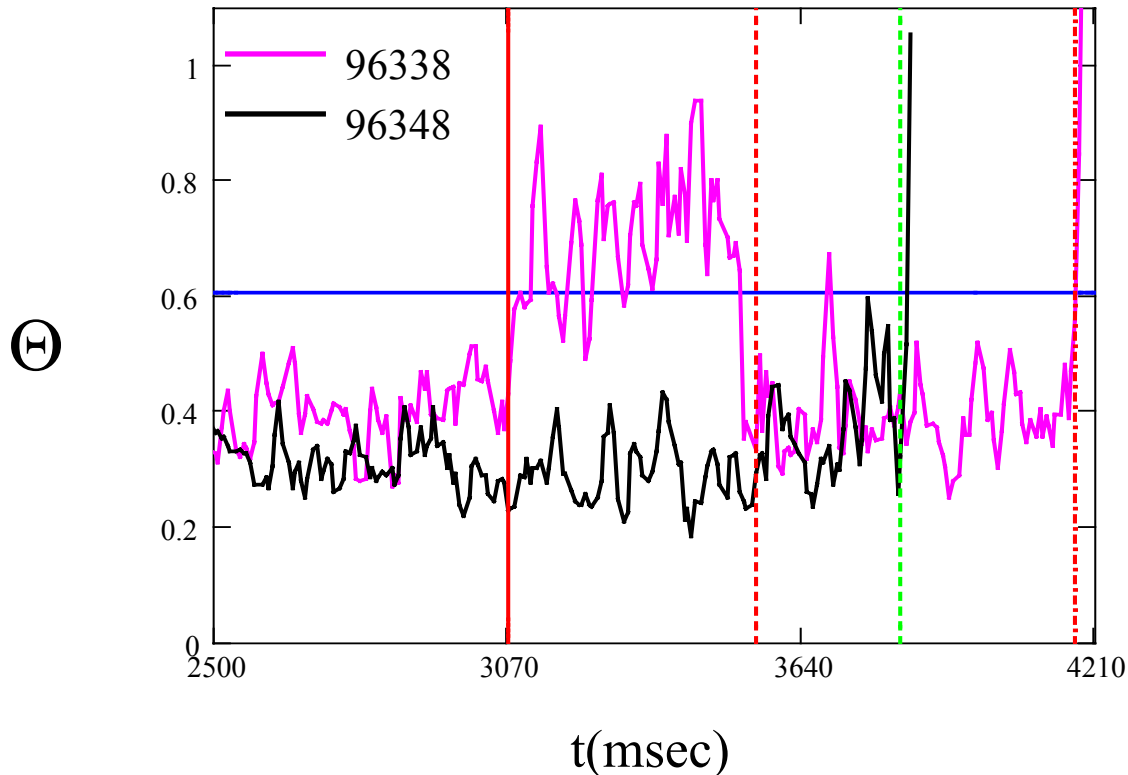
COMPARISON WITH DIII-D GRAD B TOWARDS AND AWAY FROM THE X POINT

$I_p=0.97$ MA, $B_T=2.12$

Shot #96338 (∇B drift to X point) —

Shot #96348 (∇B drift away X point) —

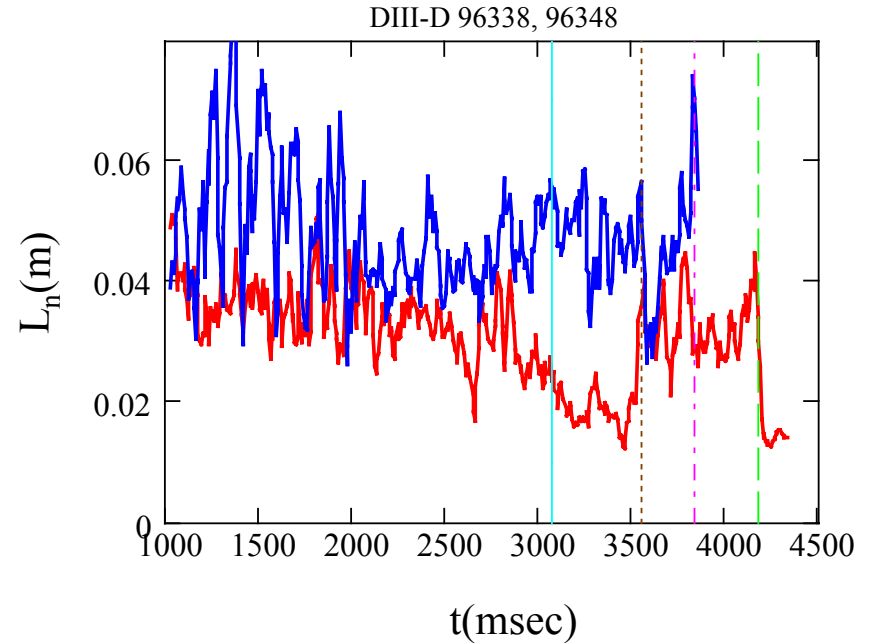
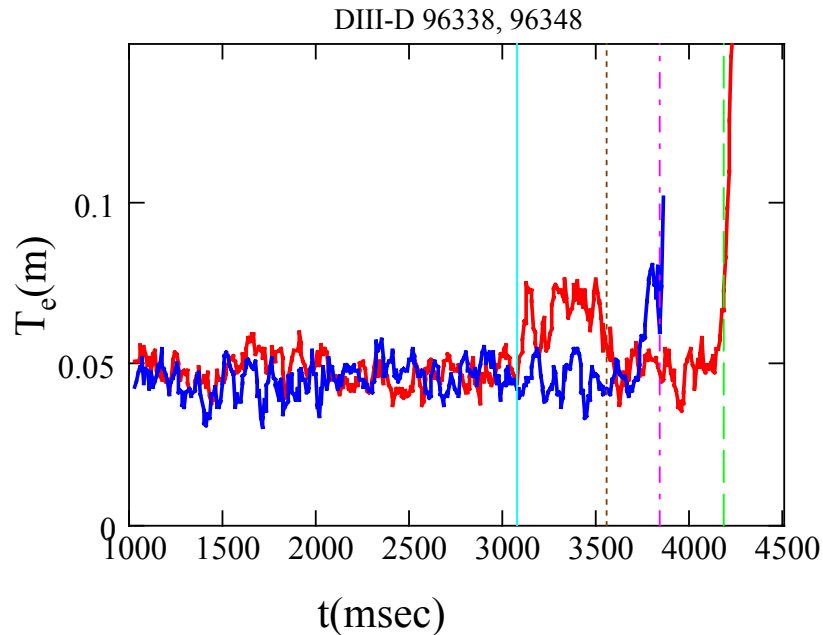
$$\Theta = \frac{T_e(\text{keV})}{\sqrt{L_n(\text{m})}}$$





COMPARISON WITH DIII-D GRAD B TOWARDS AND AWAY FROM X POINT

Shot #96338 (∇B drift to X point) ————
Shot #96348 (∇B drift away X point) ————





CONNOR AND POGUTSE, PHYS PLASMAS CNTRL FUSION 43, 281, 2001

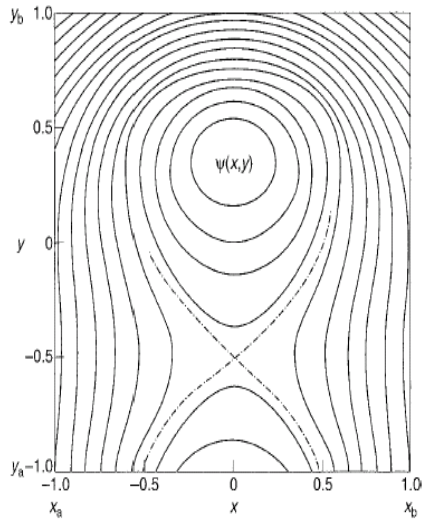


Figure 8. The magnetic flux function for the two-wire model used in the computational model of appendix B.

$$\frac{\partial}{\partial t} T_0(x, y, t) + \text{div}(\vec{q}_i(x, y, t)) = Q(x, y)$$

where the thermal flux includes the drift term, transverse and parallel terms:

$$\vec{q}_i(x, y, t) = -V_{i0}\vec{e}_y T_0(x, y, t) - \chi_{\perp i} \nabla_{\perp} T_0(x, y, t) - \chi_{\parallel i} \vec{b}(\vec{b} \cdot \nabla) T_0(x, y, t)$$

$$\frac{\partial}{\partial t} n_e(x, y, t) + \text{div}(\vec{\Gamma}_e(x, y, t)) = C_i n_0(x, y, t) n_e(x, y, t)$$

$$\vec{\Gamma}_e(x, y, t) = -V_{e0}\vec{e}_y n_e(x, y, t) - D_{\perp e} \nabla_{\perp} n_e(x, y, t) - D_{\parallel e} \vec{b}(\vec{b} \cdot \nabla) n_e(x, y, t)$$

$$\frac{\partial}{\partial t} n_0(x, y, t) + \text{div}(\vec{\Gamma}_0(x, y, t)) = -C_i n_0(x, y, t) n_{e0}(x, y, t)$$

$$\vec{\Gamma}_0(x, y, t) = -D_0 \nabla n_0(x, y, t).$$



CONNOR AND POGUTSE, PHYS PLASMAS CNTRL FUSION 43, 281, 2001

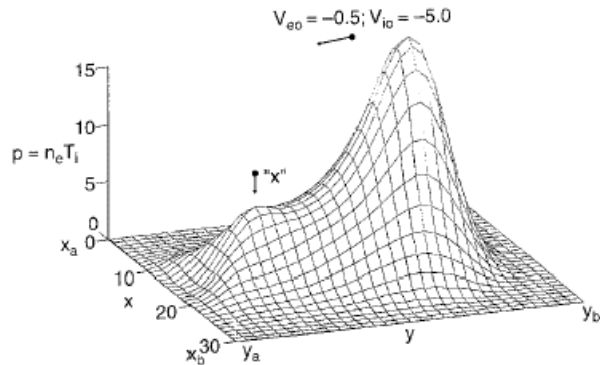


Figure 14. The two-dimensional surface of the pressure, $p = n_e T_i$, for the drift towards the X-point: $V_{i0} = -5.0$ and $V_{e0} = -0.5$. The density profile enhances the X-point effect.

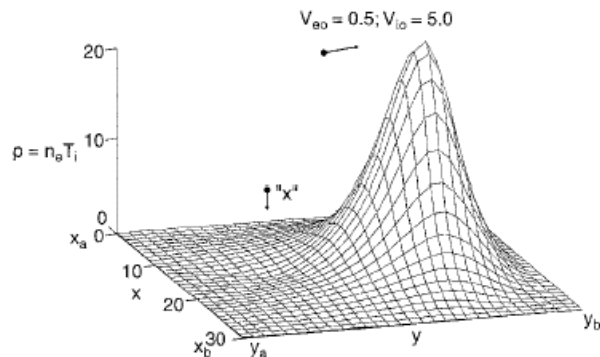
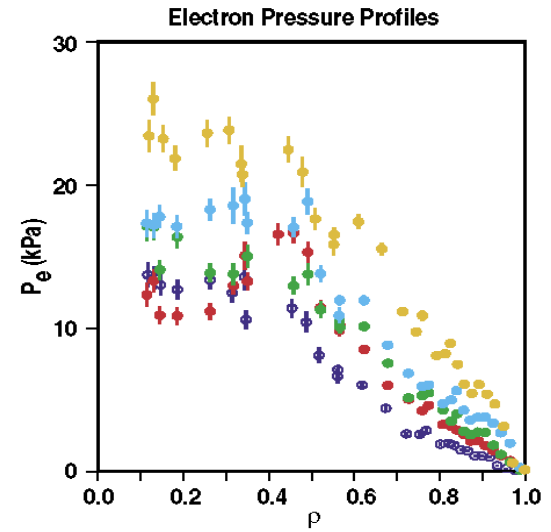
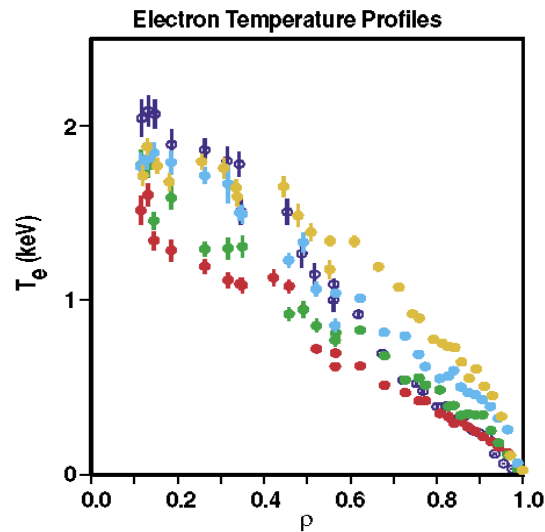
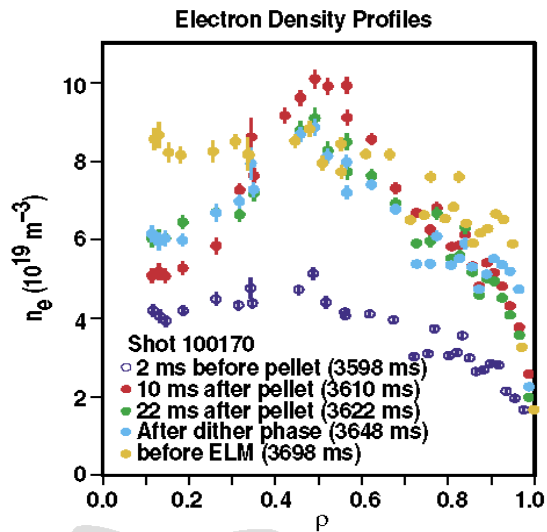
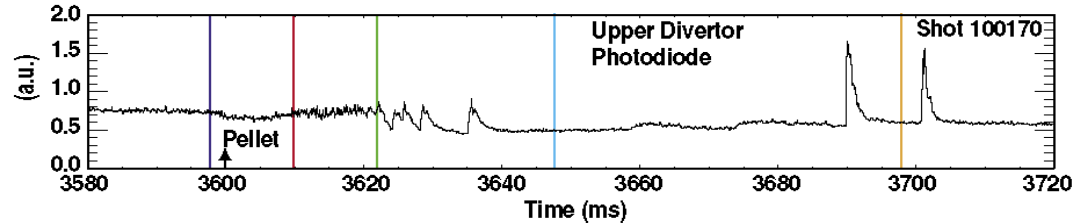


Figure 15. The two-dimensional surface of the pressure, $p = n_e T_i$, for the drift away from the X-point: $V_{i0} = 5.0$ and $V_{e0} = 0.5$.

Grad B drift towards X-point leads to steeper pressure gradient on in the mid-plane



GOHIL ET AL. PHY. REV LETT. 86, 644 (2001)

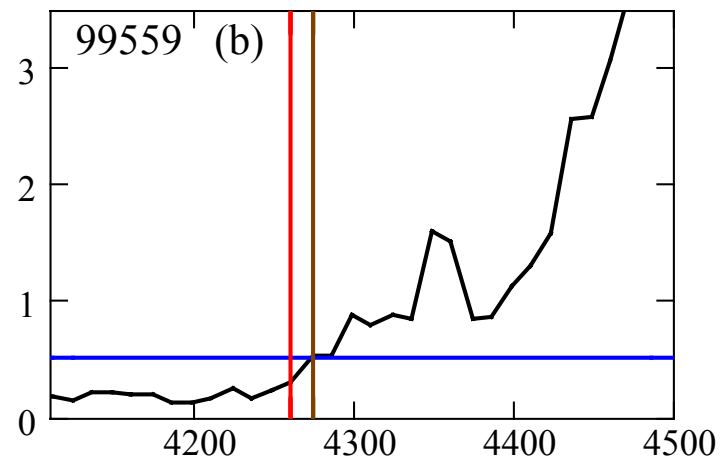
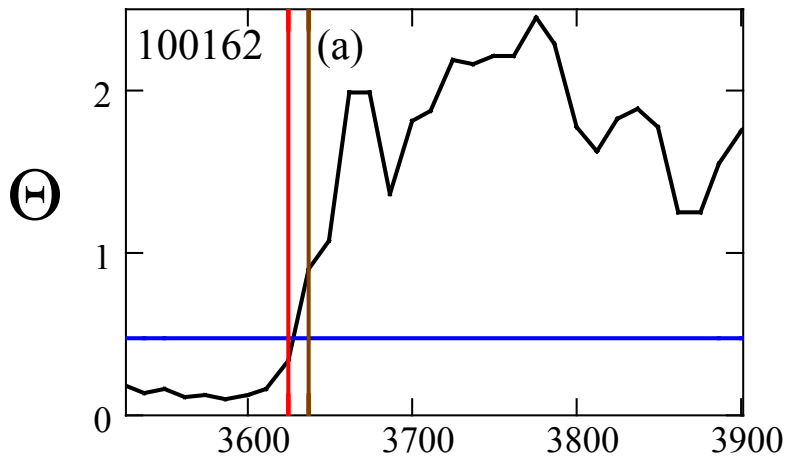


Strong reduction in L_n in the edge 2 msec prior to transition



COMPARISON WITH DIII-D WITH PELLETT SHOTS 100162, 99559

Pellet Induced H mode





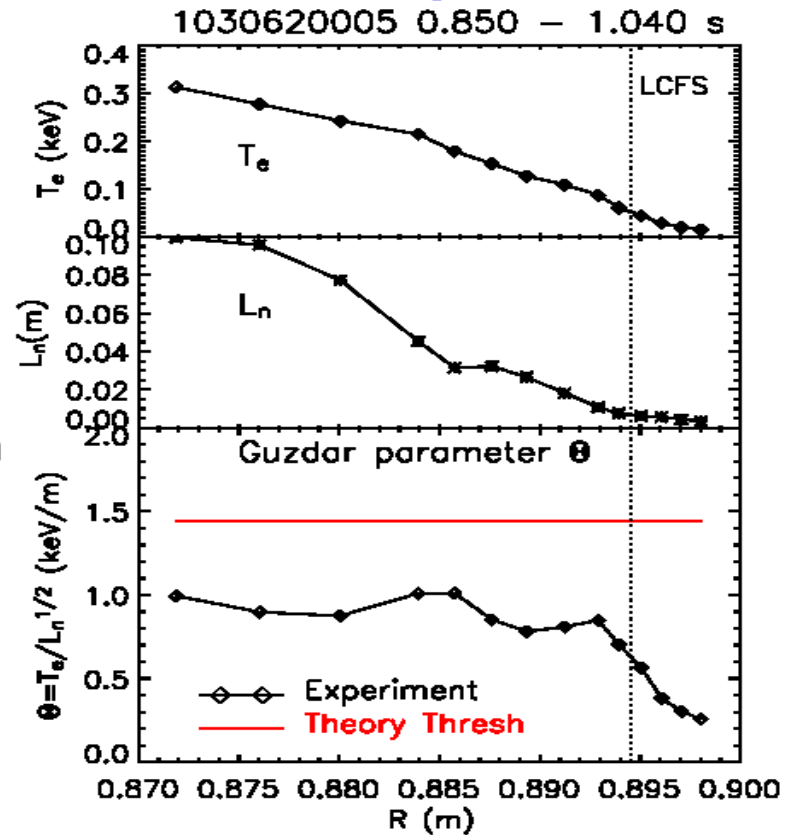
COMPARISON WITH C-MOD

AMANDA HUBBARD, MIT, PSFC

9th IAEA H-MODE WORKSHOP, SAN DIEGO,

Theory/Experiment Comparison

- Use the averaged TS profiles shown above, with 3-pt radial smoothing.
- For consistency with DIII-D evaluation, used central value of B_T (6.1 T) and $Z_{\text{eff}} = 1$ (Experimental $Z_{\text{eff, av}}$ was 1.8).
- Guzdar recommends evaluating a point of maximum n_e gradient. However, for C-Mod this usually occurs near the separatrix where T_e is low and shows little variation. We therefore evaluate $\Theta(r)$ across the edge profile.





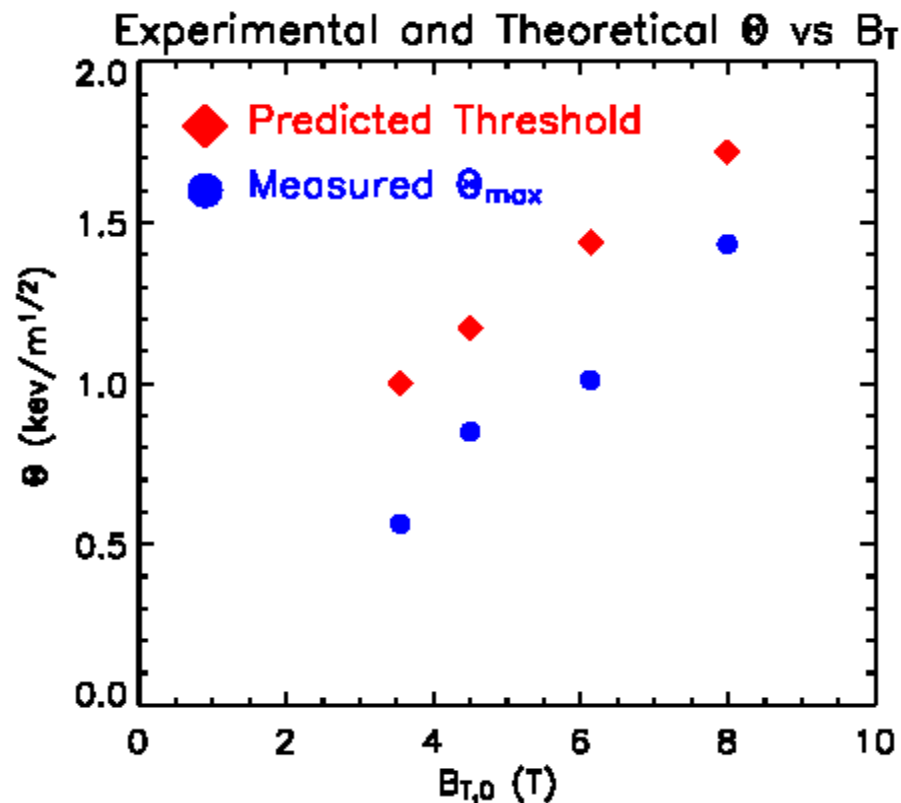
COMPARISON WITH C-MOD

AMANDA HUBBARD, MIT, PSFC

9th IAEA H-MODE WORKSHOP, SAN DIEGO,

Θ increases with B_T

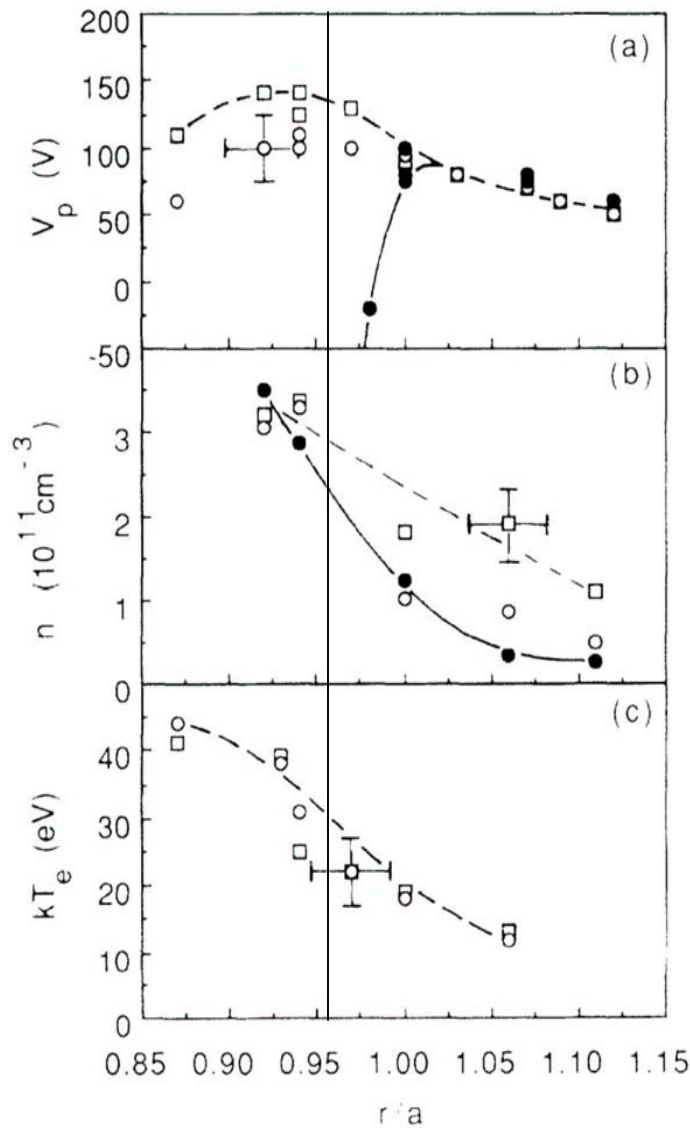
- A few other non-dedicated discharges with long steady or dithering pre-LH periods, with B_T ranging from 3.6 (ohmic H-mode) to 8 T were analysed.
- Experimental Θ_{\max} is consistently slightly below Θ_c , indicating **the predicted B_T scaling is approximately correct.**
- More data are required to determine the exponent accurately.





Electric Field Induced H-mode in CCT

Tynan et al. PRL 68,3032 (1992)



Continuous Current Tokamak
 $I_p=38\text{KA}$, $B_T=0.25\text{T}$, $R=1.48$
 $a=0.36\text{m}$

FIG. 1. (a) Plasma potential, (b) equilibrium density, and (c) electron temperature profiles on the outside midplane region during Ohmic L -mode phase (□), with injected current on but prior to bifurcation (○), and during the H -mode confinement regime (●). The density profile steepens and a strong radially inward electric field develops during the H -mode transition.

Probe potential and radial electric field modifies the equilibrium density to set up condition for self-consistent zonal flow to develop spontaneous transition.

$L_n=0.27 \text{ m}$, $Z_{\text{eff}}=2.0$ $T_{\text{ec}}=30 \text{ eV}$



CONCLUSIONS AND FUTURE WORK

- Derived generalized dispersion relation for shear/zonal flow with finite beta effects.
- Theory gives reasonable preliminary agreement with simulations and data on DIII-D and C-MOD

Future work

- undertake more careful study of the nonlocal dispersion relation
- study the low-dimensional nonlinear equations with finite beta to understand nature of the H mode attractor
 - fixed point (non-ELMing),
 - chaotic (ELMing)
- current theory is in terms of plasma parameters (T_e , T_i , L_n) and not in terms of true control parameters. Use this simple expression in 1D and 2D predictive transport codes To obtain threshold power dependence and then make predictions for future devices
- Extend theory to core enhanced confinement modes